A MATHEMATICAL STUDY OF THE EFFECT OF A MOVING BOUNDARY AND A THERMAL BOUNDARY LAYER ON DROPLET HEATING AND EVAPORATION

IVAN GUSEV

PHD 2012

A MATHEMATICAL STUDY OF THE EFFECT OF A MOVING BOUNDARY AND A THERMAL BOUNDARY LAYER ON DROPLET HEATING AND EVAPORATION

IVAN GUSEV

A thesis submitted in partial ful lment of the requirements of the University of Brighton for the degree of Doctor of Philosophy

January 2012

Sir Harry Ricardo Laboratories
The University of Brighton

Abstract

Two new solutions to the heat conduction equation, describing transient heating of an evaporating droplet, are suggested. Both solutions take into account the effect of the reduction of the droplet radius due to evaporation, assuming that this radius is a linear function of time. It has been pointed out that the new approach predicts lower droplet surface temperatures and slower evaporation rates compared with the traditional approach. New solutions to the heat conduction equation, describing transient heating of an evaporating droplet, are suggested, assuming that the time evolution of droplet radius $R_d(t)$ is known. The results of calculations are compared with the results obtained using the previously suggested approach, when the droplet radius was assumed to be a linear function of time during individual time steps, for typical Diesel engine-like conditions. Both solutions predict the same results which indicates that both models are likely to be correct.

Two new solutions to the equation, describing the diffusion of species during multi-component droplet evaporation, are suggested. The first solution is the explicit analytical solution to this equation while the second one reduces the solution of the differential species diffusion equation to the solution of the Volterra integral equation of the second kind. Both solutions take into account the effect of the reduction of the droplet radius due to evaporation, assuming that this radius is a linear function of time. The analytical solution has been incorporated into a zero dimensional CFD code and applied to the analysis of bi-component (50% ethanol – 50% acetone mixture) droplet evaporation at atmospheric pressure.

The transient heat conduction equation, describing heating of a body immersed into gas with inhomogeneous temperature distribution, is solved analytically, assuming that, at a certain distance from the body, gas temperature remains constant. The solution is applied to modelling of body heating in conditions close to those observed in Diesel engines. In the long time limit, the distribution of temperature in the body and gas practically does not depend on the initial distribution of gas temperature.

Contents

List of Tables

List of Figures

4.6 The time evolution of droplet surface temperatures (T_s) and radius (R_d), predicted by the one-way Solution A for the non-ideal model, taking and not taking into account the e ects of the moving boundary

Acknowledgements

First of all I would like to thank my supervisors Prof. Sergei Sazhin and Prof. Morgan Heikal for their support during my work on this project. Also I am grateful to Dr. Pavel Krutitskii, Dr. Michael Vynnycky, Dr. Sarah Mitchell, Dr. Elena Sazhina, Dr. Guillaume Castanet, Prof. Fabrice Lemoine and Mr. Ahmed Elwardany for their criticism, support and valuable contributions to this work.

Last, but not least, I would like to thank my family and friends who gave me much inspiration and a moral boost.

Finally I am grateful to the European Regional Development Fund Franco-British INTERREG IVA (Project C5, Reference 4005) for the nancial support of this project.

Declaration

Nomenclature

$a; b$	coe cients introduced in Equation (2.7) or $1 = \sqrt{\ }$
$a_{b;g}$	coe cients introduced in Eq. (5.9) ($\sqrt{s}$/m)
b	weight (see Appendix 7) [J/(m^3 K)]
A	function de ned by Eq. (A711)
B	function de ned by Eq. (A711)
B_M	Spalding mass transfer number

p	pressure [Pa] or parameter introduced in Equation (4.23)
p	

W	function introduced by Equation (2.17) or (4.14)
X	molar fraction
Y	mass fraction

Greek symbols

	evaporation rate introduced in Equation (2.8)
$_m$	parameter de ned by Equation (4.3)
$_{T0}$	thermal ` lm' thickness [m]
	$(t_{e\ (new)}\quad t_{e\ (conventional)})=t_{e\ (new)}$
t	time step [s]
T	$T_g \quad T_s$ [K]
	activity coe cient
	evaporation rate
	function de ned by Equation (2.25) or (A61) or (4.22)
$_s$	$\frac{T_s \quad T_0}{T}$
	function de ned by Equation (4.44)
	thermal di usivity (m^2/s)
$,\ _n$	eigenvalues de ned by Equations (2.28),(4.26),(4.28) or (5.11)
(t)	variable introduced by Equation (2.13) or (4.18)
$\hat{}_0(t)$	variable introduced in Equation (4.49)
(t)	function de ned by Equation (3.5) or kinematic viscosity
$!(t;\ )$	function de ned in Appendix 3
$(t;\ )$	function de ned in Appendix 3
	$R=R_d(t)$
	parameter de ned by Eq. (5.19)
$_Y$	parameter de ned by Equation (4.6)
	density [kg/ m^3]
(t)	$W(t;1)$

Subscripts

a	air
amb	ambient

b	body or boiling
d	droplet
e	evaporation
eff	e ective
eth	ethanol
f	fuel
g	gas
i	species
iso	isolated
l	liquid
n	timesteps in the integration
p	constant pressure
part	particular
s	surface
v	vapour
0	initial
1	ambient conditions

Chapter 1

Introduction

1.1 Motivation

heat conduction equation inside droplets. It was shown that this approach is more e cient, compared with the one based on the numerical solution to this equation, both from the point of view of accuracy and of CPU e ciency [16].

1) models based on the assumption that the droplet surface temperature is uniform and does not change with time;

2) models based on the assumption that there is no temperature gradient inside droplets (infinite thermal conductivity of liquid);

3) models taking into account finite liquid thermal conductivity, but not the re-circulation inside droplets (conduction limit);

4) models taking into account both finite liquid thermal conductivity and the re-circulation inside droplets via the introduction of a correction factor to the liquid thermal conductivity (effective conductivity models);

5) models describing the re-circulation inside droplets in terms of vortex dynamics (vortex models);

alternative approach was suggested and developed in [1, 15{17, 52]. In these papers both nite liquid thermal conductivity and recirculation inside droplets (via the e ective thermal conductivity (ETC) model [44]) were taken into account by incorporating the analytical solution to the heat conduction equation inside the droplet into a numerical scheme. The liquid thermal conductivity inside droplets was replaced by the e ective thermal conductivity to take into account liquid recirculation assumption that species inside droplets mix infinitely quickly. Models containing features of both these groups of models have been suggested in [66]. Most of the models belonging to the first group are based on the numerical solution to the species diffusion equation inside droplets. At the same time the analysis of [38, 50] was based on the analytical solution to this equation. The model in [38] was applied to the analysis of heating and evaporation of bi-component ethanol/acetone droplets. The authors of [38] based their analysis on the analytical solution to the species diffusion equation, which was incorporated into the numerical code. This approach is expected to be more CPU efficient and accurate compared with the one based on the conventional approach [50]. The model described in [38] has been generalised in [50] to take into account coupling between droplets and gas. None of these models took into account the effects of the moving boundary due to evaporation on the species diffusion equation.

Most of the models of droplet heating and evaporation suggested so far are based on the assumption that gas in computational cells is always homogeneous and the gas temperature in the immediate vicinity of the droplet surface is the same as in the rest of the cell [1, 37]. The droplet heating in this case is described based model described in [67]. The latter model is based on an approach which differs from the one used in [52]. One of the main limitations of the model described in [52] is that it was based on the assumption that initially gas temperature was homogeneous in the whole domain. This imposes a serious limitation for practical applications of this model in a realistic environment when the ambient temperature can vary with time.

Near-critical and supercritical droplet heating and evaporation was covered in relatively recent reviews [68, 69], and [64]. Analysis of the interaction between droplets, collisions, coalescence, atomization, oscillations (including instabilities of evaporating droplets) and size distribution were considered in [70–85]). The problem of heating and evaporation of droplets on heated surfaces was considered in [82, 86]. The problem of droplet heating and evaporation is related to spray combustion (see [9, 10, 87–89]). Two groups of models for radiative heating of droplets have been considered: the one based on the assumption that droplets are opaque grey spheres [42, 47, 90], and the one based on the assumption that droplets are semi-transparent for thermal radiation [91–97]. The first approach is the one used in all CFD codes which are known to us, while the second one is much more appropriate from the point of view of underlying physics. The Soret effect describes the flow of matter caused by a temperature gradient (thermal diffusion), while the Dufour effect describes the flow of heat caused by concentration gradients. The two effects occur simultaneously. Both effects are believed to be small in most cases although sometimes their contribution may be significant (see [98–102]). Kinetic and molecular dynamics effects on droplet heating and evaporation were considered in [2–5, 7, 103, 104]. All effects mentioned in this paragraph will be ignored in our analysis.

1.3 Structure of the thesis

In Chapter 2 a model for mono-component droplet heating and evaporation, based on the assumption that droplet radius is a linear function of time during time steps, is presented and discussed. A more general model, based on the assumption that droplet radius is an *a priori* known function of time, is discussed in Chapter 3.

In Chapter 4 the effects of the moving boundary on the solution to the species diffusion equation in multi-component droplets are discussed. A model for body heating/cooling, when this body is immersed into an ambient gas with temperature varying with distance from the surface of the body, is presented in Chapter 5. The main results of the thesis are summarised in Chapter 6.

Chapter 2

Transient heating of an evaporating droplet when droplet is a linear function of time

2.1 Introduction of Chapter 2

Taking into account the effect of receding droplet radius on droplet heating and evaporation leads to the well known Stefan problem, which has been widely discussed in the literature (e.g. [105]-[54]), but has been rarely applied to engineering sprays, due to the complex structure. Hence, a substantial gap has developed between mathematical and engineering research in this field. The main objective of this work is to fill this particular gap. This will include the development of an appropriate mathematical model for specific spray applications, and the actual application of this model to simulate droplet heating and evaporation processes in Diesel engine-like conditions. There has been no previous research in this direction to the best of our knowledge.

The essence of the difference between the new approach to the modelling of droplet heating and evaporation, suggested in this chapter, and the traditional approach is schematically illustrated in Fig. 2.1. As follows from this figure, the approximation of the reduction of the droplet radius during the time step by the linear function is noticeably much more accurate than the approximation based on the assumption that the droplet radius is constant during the time step (the conventional approach

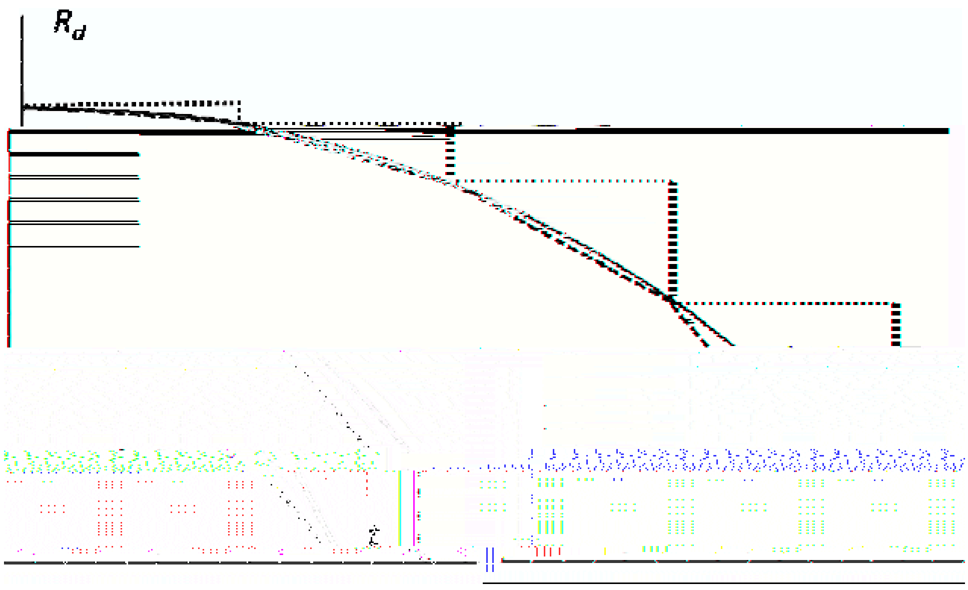

Figure 2.1: A schematic presentation of the plot R_d versus t for an evaporating droplet (solid); approximation of this plot using the conventional approach assuming that R_d = const during the time step (dotted); approximation of this plot using the new approach assuming that R_d is the linear function of t during each time step (dashed).

used in CFD codes). This di erence, however, can be mitigated by choosing su - ciently small time steps (more time steps would be required in the case when the reduction of droplet radius during the time step is ignored than in the case when it is taken into account). A more important implication of the new approach, compared with the traditional one, however, is that the e ect of the reduction of droplet radius on droplet heating is explicitly taken into account in the new approach at every time step. This leads to the prediction of temperatures di erent compared with the ones predicted by the traditional approach, regardless of how many time steps are used in the analysis. These di erences in droplet temperatures lead to di erent time dependencies of droplet radii. These e ects will be illustrated in this chapter using examples of fuel droplet heating and evaporation in Diesel engine-like conditions.

The basic equations and approximations of the new model are described in Section 2. The analysis and solutions of these basic equations are given in Section 3. In Section 4, one of these solutions is analysed for the values of parameters typical for Diesel engines. The main results of the chapter are summarised in Section 5.

2.2 Basic equations and approximations

Let us assume that an evaporating droplet is immersed into a homogeneous hot gas at constant temperature T_g. The droplet is heated by convection, with the convection heat transfer coefficient $h(t)$ depending on time t and droplet radius $R_d(t)$, and cools down due to evaporation. $R_d(t)$ is a continuously differentiable function of time in the range $0 \leq t \leq t_e$, where t_e is the evaporation time. Both $R_d(t)$ and $h(t)$ are assumed to be known. Effects of thermal radiation are taken into account. The changes in the droplet temperature ($T \equiv T(t; R)$) are described by the heat conduction equation in the form [105, 106]:

$$\frac{\partial T}{\partial t} = \kappa \left(\frac{\partial^2 T}{\partial R^2} + \frac{2}{R} \frac{\partial T}{\partial R} \right) + P(R) \tag{2.1}$$

for $0 \leq t < t_e$, $0 \leq R < R_d(t)$, where κ is liquid thermal diffusivity ($\kappa = k_l/(c_l \rho_l)$ =const), k_l is the liquid thermal conductivity, c_l is the liquid specific heat capacity, ρ_l is the liquid density, R is the distance from the centre of the droplet.

The term $P(R)$ takes into account the effects of thermal radiation, assuming that droplets are semi-transparent (radiation can penetrate inside droplets). Various approximations for $P(R)$ were suggested in [91]–[107].

Remembering the physical background of the problem, we look for the solution of this equation in the form of a twice continuously differentiable function $T \equiv T(t; R)$ for $0 \leq t < t_e$, $0 \leq R < R_d(t)$. This solution should satisfy the boundary condition:

$$\left. \left(k_l \frac{\partial T}{\partial R} + hT \right) \right|_{R=R_d(t)} = hT_g + \rho_l L \dot{R}_d(t); \tag{2.2}$$

T is finite and continuous at $R \to +0$, $T_s = T(R_d(t); t)$ is the droplet's surface temperature, L is the specific heat of evaporation. We took into account that $\dot{R}_d(t) \equiv \mathrm{d}R_d/\mathrm{d}t \leq 0$. Effects of swelling are ignored. Equation (2.2) is just the energy balance condition at $R = R_d(t)$. The initial condition is taken in the form:

$$T(t = 0) = T_0(R); \tag{2.3}$$

where $0 \leq R \leq R_{d0} = R_d(t = 0)$.

The value of $R_d(t)$ is controlled by fuel vapour diffusion from the droplet surface, and can be found from the equation [1]:

$$\dot{R}_d = -\frac{k_g \ln(1 + B_M)}{\rho_l c_{pg} R_d}; \tag{2.4}$$

where

$$B_M = \frac{Y_{vs} \quad Y_{v1}}{1 \quad Y_{vs}}; \tag{2.5}$$

is the Spalding mass transfer number, Y_{fs} is the mass fraction of fuel vapour near the droplet surface:

$$Y_{fs} = \left[1 + \left(\frac{p}{p_{fs}} \quad 1\right)\frac{M_a}{M_f}\right]^{1}; \tag{2.6}$$

Y_{v1} is the mass fraction of fuel vapour in ambient gas (in our analysis we assume $Y_{v1} = 0$),

p and p_{fs} are ambient pressure and the pressure of saturated fuel vapour near the surface of the droplet respectively, M_a and M_f are molar masses of air and fuel; p_{fs} is calculated from the Clausius-Clapeyron equation presented in the form:

$$p_{fs} = \exp\left[a \quad \frac{b}{T_s \quad 43}\right]; \tag{2.7}$$

a and b are constants to be speci ed for speci c fuels, T_s is the surface temperature of fuel droplets in K; p_{fs} predicted by Equation (2.7) is in kPa.

In [15] it was assumed that R_d =const, while the contribution of $\dot{R}_d$ was taken into account by replacing gas temperature with the so called e ective temperature. It was assumed that this approach is applicable when used during relatively short times (time steps in computational uid dynamics (CFD) codes), but it has never been rigorously justi ed. The focus of this chapter is on the e ects of changing droplet radius during the time step on the heating of droplets.

The current state of the development of mathematical tools for the solution of this type of problem is described by Kartashov [105]. In the following analysis, some of the results described in [105] will be adapted to the investigation of our problem.

A number of simplifying assumptions will be made. Firstly, the contribution of thermal radiation will be ignored ($P(R) = 0$). Secondly, we assume that $R_d(t)$ is the linear function of t:

1" 0 Td [(kls,)]TJ/F22 11.9552 T08910.617 0 Td [gT(fIn 1167[(d)]
$R_d(t)$ J/F18 11.9552 Tf 4.855 1.793 Td :]TJ/F22 11.9552 Tf 7.
B

108]. As follows from the analysis of [96], in the case when external temperature, responsible for radiative heating, is about or less than 1000 K the effect of radiation on droplet evaporation is less than about 1% (see Fig. 2.3 of [96]). This justifies our assumption that $P(R) = 0$.

The second assumption is justified if the results are applied to a relatively short period of time, when $R_d(t)$ can be expanded into a Taylor series in time and only the first two terms are retained (in our previous analyses and in all CFD codes known to us, only the zeroth terms were used). In this case, $t = 0$ will refer to the beginning of the time step t_0, t_e will refer to $t_0 + \Delta t$, where Δt is the time step.

Note that Brenn [54], considering a different problem of calculating the concentration field in evaporating droplets, assumed that R_d^2, rather than R_d, is a linear function of time during the whole evaporation process:

$$R_d^2(t) = R_{d0}^2 - \beta' t. \tag{2.10}$$

This could be justified by Eq. (2.4) assuming that B_M = const. In our case this assumption can be made during the time step but not during the whole evaporation process. For sufficiently small time steps, both approaches lead to identical results since:

$$R_d = R_{d0}\sqrt{1 - \beta' t / R_{d0}^2} \approx R_{d0}(1 + \alpha t);$$

where $\alpha = -\beta'/(2R_{d0}^2)$.

The problem considered in [54] is more general compared with the one considered in this chapter, as the 3D effects on species concentrations were taken into account in that paper. If only the radial dependence of this concentration is taken into account, Eq. (1) of [54] would have exactly the same structure as Eq. (2.1) in this chapter. However, the solution of his equation cannot be used for our equation due to different boundary conditions used in our papers.

Among other assumptions used in our analysis we mention that the effects of the interaction between droplets were ignored. This can be justified when the distance parameter (ratio of the distance between droplets to their diameters) is large (see [49] for details).

2.3 Analysis of the equations

2.3.1 Preliminary analysis

Let us rewrite boundary condition (2.2) in the form:

$$\frac{\partial T}{\partial R} + h$$

we can rewrite Equation (2.12) as

$$R_d^2(t)F'_t = \quad F'' + \quad R'_d(t)R_d(t)F' : \tag{2.16}$$

Equation (2.16) is identical to the one studied in [109], where the distribution of temperature in the melting region was considered (plane problem).

Equation (2.16) is to be solved at $t \in [0; t_e]$ (or $t \in [t_0; t_0 + \quad t]$) and $0 \quad\quad 1$. Initial and boundary conditions for this equation can be presented as:

$$F|_{t=0} = R_{d0} \ T_0(\ R_{d0}); \quad 0 \quad\quad 1;$$

$$F|_{\ =0} = 0; \qquad F' + \bar{H}(t)F|_{\ =1} = \tilde{\ }(t); \quad 0 \quad t \quad t_e \quad (\text{or } t \in [t_0; t_0 + \quad t]);$$

where $\bar{H}(t) = H(t)R_d(t)$, $\tilde{\ }(t) = M(t)R_d^2(t)$.

Following Kartashov [105], we introduce the new unknown function $W(t; \ )$ via the relation:

$$F(t; \ ) = \frac{1}{\sqrt{R_d(t)}} \exp\left[\quad \frac{R'_d(t)R_d(t)}{4} \ ^2 \right] W(t; \ ): \tag{2.17}$$

From Equation (2.17) we obtain the following expressions for the derivatives:

$$F'_t = \left(\left[\quad \frac{1}{2}R_d^{\ 3/2}(t)R'_d(t) + R_d^{\ 1/2}(t) \left(\quad \frac{(R'_d(t))^2 + R_d(t)R''_d(t)}{4} \ ^2 \right) \right] W(t; \ ) \right.$$

$$\left. + R_d^{\ 1/2}(t)W'_t(t; \ ) \right) \exp\left[\quad \frac{R'_d(t)R_d(t)}{4} \ ^2 \right];$$

$$F' = \left\{ \quad \frac{2 \ R'_d(t)R_d(t)}{4 \sqrt{R_d(t)}} W(t; \ ) + \frac{1}{\sqrt{R_d(t)}} W'(t; \ ) \right\} \exp\left[\quad \frac{R'_d(t)R_d(t)}{4} \ ^2 \right];$$

$$F'' = \left\{ \frac{2}{\sqrt{R_d(t)}} \left[\quad \frac{R_d(t)R'_d(t)}{4} \right. \right.$$

lss1 9.9626 Tf 19.i

In the case of non-zero d^2R_d/dt^2 and $P(R)$, Eq. (2.18) would need to be replaced by the following equation (cf. Equation (8.149) in [105]):

$$R_d^2(t)W_t'(t;\ ) = W''(t;\ ) + \left[\frac{\ ^2}{4} R_d^3\frac{d^2R_d}{dt^2}\right]W(t;\ ) + \frac{R_d^2 R}{q_K(\ ;t)}P(R); \qquad (2.19)$$

where

$$q_K(\ ;t) = \sqrt{\frac{1}{R_d(t)}}\exp\left[\frac{R_d'(t)R_d(t)}{4}\ ^2\right]:$$

Equation (2.19) reduces to Equation (2.18) in the limit when $d^2R_d/dt^2 = 0$ and $P(R) = 0$.

Equation (2.18) is to be solved subject to initial and boundary conditions:

$$W(t;\ )|_{t=0} = W_0($$

The solution to Equation (2.28) gives a set of positive eigenvalues $_n$ numbered in ascending order ($n = 1; 2; \ldots$). If $h_0 = 0$, then $_n = \;(n \;\; \frac{1}{2})$. Assuming that $B = 1$, expressions for eigenfunctions $v_n(\;)$ can be written as:

$$v_n(\;) = \sin \;_n \qquad (n = 1; 2; \ldots). \tag{2.29}$$

The solution $\;= 0$ is excluded as it leads to a trivial solution $v_n(\;) = 0$.

The value of B is implicitly accounted for by the coe cients $_n(t)$ in Series (2.25). The functions $v_n(\;)$ form a full set of eigenfunction functions which are orthogonal for $\;2\; [0; 1]$. The orthogonality of functions $v_n(\;)$ follows from the relation:

$$\int_0^1 v_n(\;)v_m(\;)\mathrm{d}\; = \;_{nm} \,||\, v_n \,||^2; \tag{2.30}$$

where:

$$_{nm} =$$

this case one can show that [15]:

$$|q_n| < \frac{\text{const}}{{}^{2}_{n}}. \qquad (2.34)$$

Remembering Equations (2.25) and (2.32), Equation (2.24) can be rewritten as:

$$\sum_{n=1}^{\infty} \left(R_d^2(t)\frac{\mathrm{d}\ {}_n(t)}{\mathrm{d}t} + {}_n(t)\ {}^{2}_{n} \right) v_n(\ ) = \sum_{n=1}^{\infty} \left(f_n R_d^2(t)\frac{\mathrm{d}\ {}_0(t)}{\mathrm{d}t} \right) v_n(\ ). \qquad (2.35)$$

Both sides of Equation (2.35) are Fourier series with respect to functions $v_n(\ )$. Two Fourier series are equal if, and only if, their coefficients are equal. This implies that:

$$R_d^2(t)\frac{\mathrm{d}\ {}_n(t)}{\mathrm{d}t} + {}_n(t)\ {}^{2}_{n} = f_n R_d^2(t)\frac{\mathrm{d}\ {}_0(t)}{\mathrm{d}t}. \qquad (2.36)$$

Equation (2.36) is to be solved subject to the initial condition:

$${}_n(0) = q_n + {}_0(0) f_n. \qquad (2.37)$$

To simplify the notation, hence-forward it is assumed that $t_0 = 0$.

The general solution to the homogeneous equation:

$$R_d^2(t)\frac{\mathrm{d}\ {}_n(t)}{\mathrm{d}t} + {}_n(t)\ {}^{2}_{n} = 0 \qquad (2.38)$$

can be presented as:

$$\ln(\ {}_n$$

$$\exp\left[\frac{{}^{2}_{n}}{R_{d0}R_d(t)}\right]\int_0^t \frac{{}_0(\ )\ {}^{2}_{n}}{R_d^2(\ )}\exp\left[\frac{{}^{2}_{n}}{R_{d0}R_d(\ )}\right]\mathrm{d}\ \Bigg) : \qquad (2.42)$$

Remembering Equations (2.40) and (2.41), the solution to Equation (2.36) can be presented as:

$$_n(t) = \ _n(0)\exp\left[\frac{{}^{2}_{n}}{R_{d0}^2}\ \frac{1}{1+\ t}\quad 1\right]$$
$$+\ f_n\int_0^t \frac{\mathrm{d}\ {}_0(\ )}{\mathrm{d}}\exp\left[\frac{{}^{2}_{n}}{R_{d0}^2}\ \frac{1}{1+\ t}\quad \frac{1}{1+}\right]\mathrm{d}\ : \qquad (2.43)$$

Remembering (2.42) and (2.37) we can write an alternative formula for $_n(t)$:

$$_n(t) = q_n\exp\left[\frac{{}^{2}_{n}t}{R_{d0}R_d(t)}\right] + f_n\ {}_0(t)$$
$$f_n\ {}^{2}_{n}\int_0^t \frac{{}_0(\ )}{R_d^2(\ )}\exp\left[\frac{{}^{2}_{n}}{R_{d0}}\ \frac{1}{R_d(t)}\quad \frac{1}{R_d(\ )}\right)\Bigg]\mathrm{d}\ : \qquad (2.44)$$

Note that $_n(t)$ in the form (2.43) satis es Equation (2.36), while $_n(t)$ in the where $_n$ are given by Equations (2.43) or (2.44).

Note that strictly speaking Equation (2.45) is an implicit function of droplet temperature since depends on droplet surface temperature T_s) see Fig. 2.2). Hence, the iteration process would be required. However, as follows from our calculations (see Figs. 2.2 and 2.4-2.6), except at the very nal stage of droplet evaporation, for su ciently small time steps, the value of T_s can be taken equal to the one obtained at the end of the previous time step. This allows us to consider Equation (2.45) as an explicit formula for $T(R)$.

2.3.3 Analysis of the general case

Let us now relax our assumption that $H_0(t)$ h_0 =const> 1 and assume that:

$$H_0(t) = h_0 + h_1(t); \tag{2.46}$$

where h_0 =const> 1. Note that many of the following equations would be greatly simpli ed in the case when $h_0 = 0$. In view of (2.46) we can rewrite the boundary condition at = 1 for Equation (2.18) in the form:

$$\left[W'(t;\ ) + h_0 W(t;\ ) \right]_{=1} = {}_0(t) \quad h_1(t) W(t;1) \quad \hat{}_0(t). \tag{2.47}$$

Assuming that $\hat{}_0(t)$ is known, we can formally use the previously obtained

$$G(t;\ ;\ ) = \sum_{n=1}^{\infty} \sin(\ _n\ ) \frac{\sin(\ _n)}{R_d^2(\ ) \| v_n \|^2} \exp\left[\ \frac{\ _n^2}{R_{d0}} \left(\frac{1}{R_d(t)} \ \frac{1}{R_d(\ )} \right) \right] :$$

Explicit expressions for f_n have been used in these formulae. Both functions $V(t;\ )$ and $G(t;\ ;\ )$ are assumed to be known.

Remembering (2.47), we can rewrite Equation (2.49) as:

$$W(t;\ ) = V(t;\ ) \quad \int_0^t [\ _0(\ ) \quad h_1(\ ) W(\ ; 1)] G(t;\ ;\ ) \mathrm{d}\ : \qquad (2.50)$$

This is an integral representation for a solution to Problem (2.18)–(2.22) for time dependent $H_0(t)$ given by Equation (2.46). For $\ = 1$, integral representation (2.50) reduces to the Volterra integral equation of the second kind for function $W(t; 1)$:

$$W(t; 1) = V(t; 1) \quad \int_0^t [\ _0(\ ) \quad h_1(\ ) W(\ ; 1)] \ldots$$

Once the solution to this equation has been found we can substitute it into integral representation (2.50) and find the required solution to the initial and boundary value problem (2.18) – (2.22). The required distribution of T is found to be:

$$T(t;R) = \frac{1}{R\sqrt{R_d(t)}}\exp\left[\frac{R_d'(t)R^2}{4\;R_d(t)}\right] W(t;R/R_d(t)). \qquad (2.56)$$

In the case when $h_1(t) = 0$ and $t \quad 1$ this solution reduces to that given by Equation (16) of [15]. Note that in the case of $h_0 = 0$ we have $_n = \; (n \quad (1/2))$ and $\|v_n\|^2 = 1/2$ in all equations.

2.4 Analysis of the solutions

As follows from the previous analysis, the importance of the effects described by the new model depends on the value of the coefficient given by Equation (2.9). The plots of versus droplet surface temperature T_s

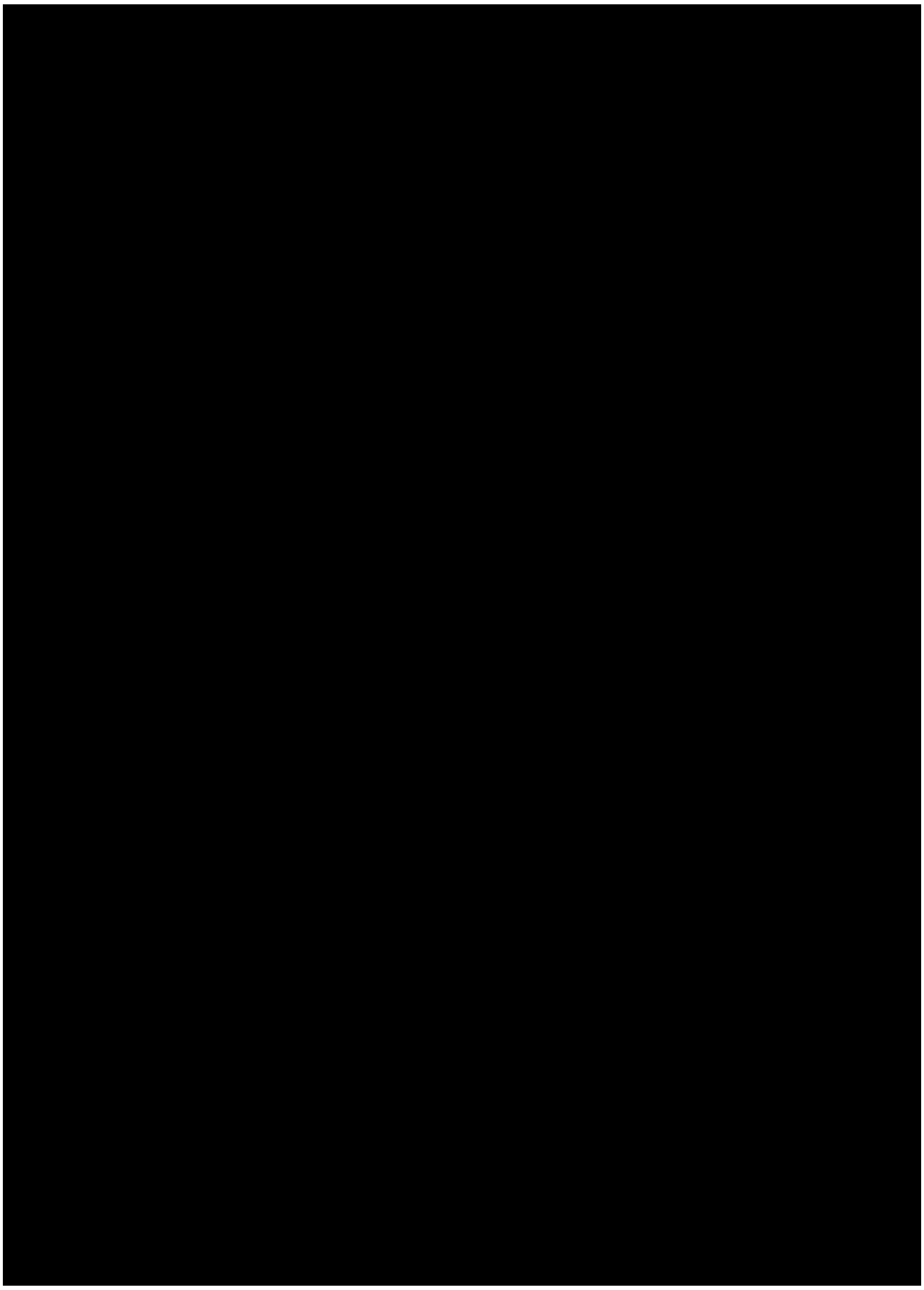

Figure 2.2: The plots of versus droplet surface temperature T_s for M_a = 29 kg/kmole, M_f = 170 kg/kmole (C_{12}

have performed similar calculations but for T_g = 2000 K (not shown). The plots without evaporation for R_{d0} =50   m in this case coincided with the ones shown in Fig. 2.2 of [15], obtained using the conventional approach.

In Fig. 2.4 we compared the results of calculations of droplet surface temperatures, taking into account the ew

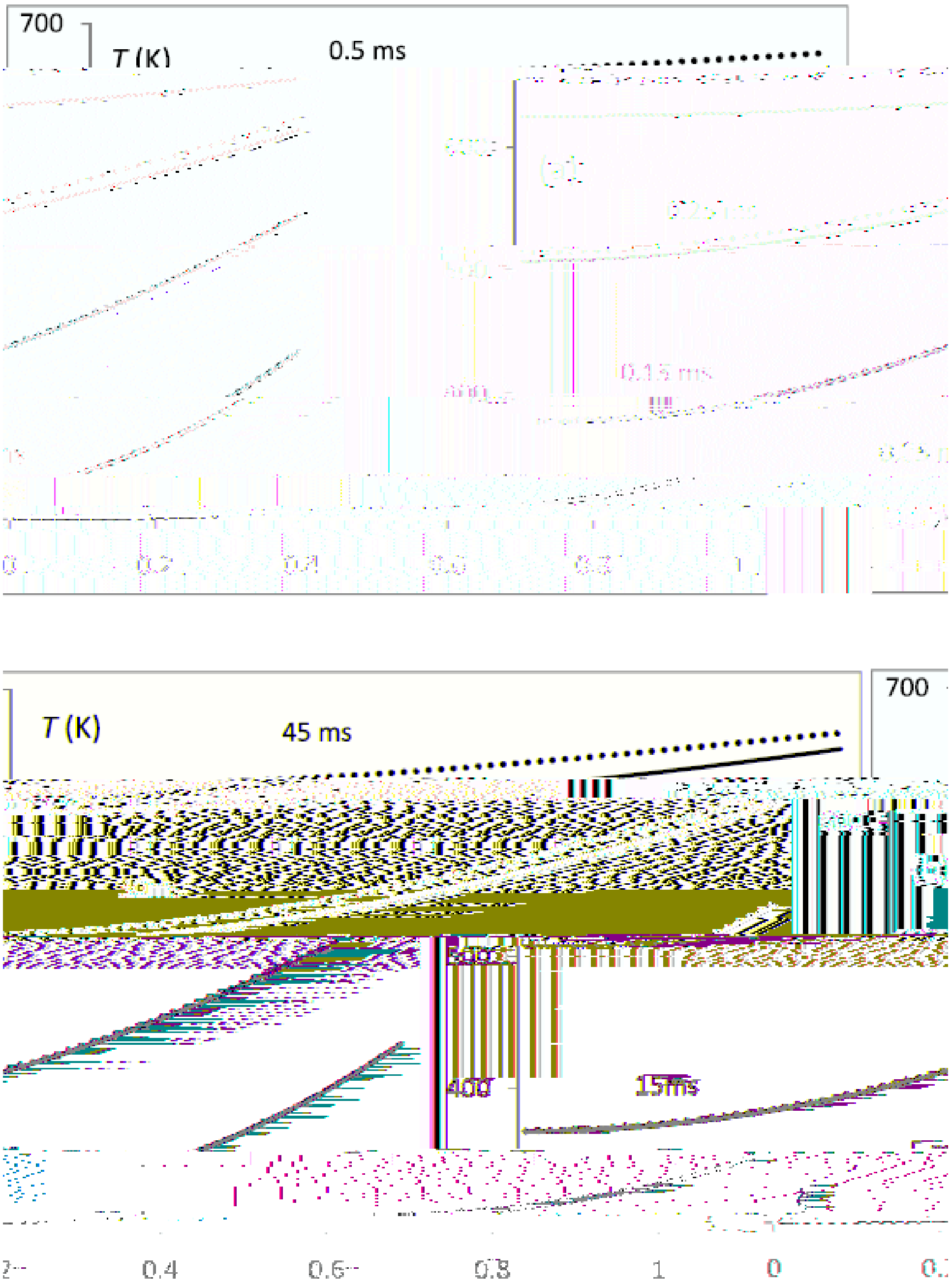

Figure 2.3: The plots of T versus $= R/R_d$ for the same values of parameters

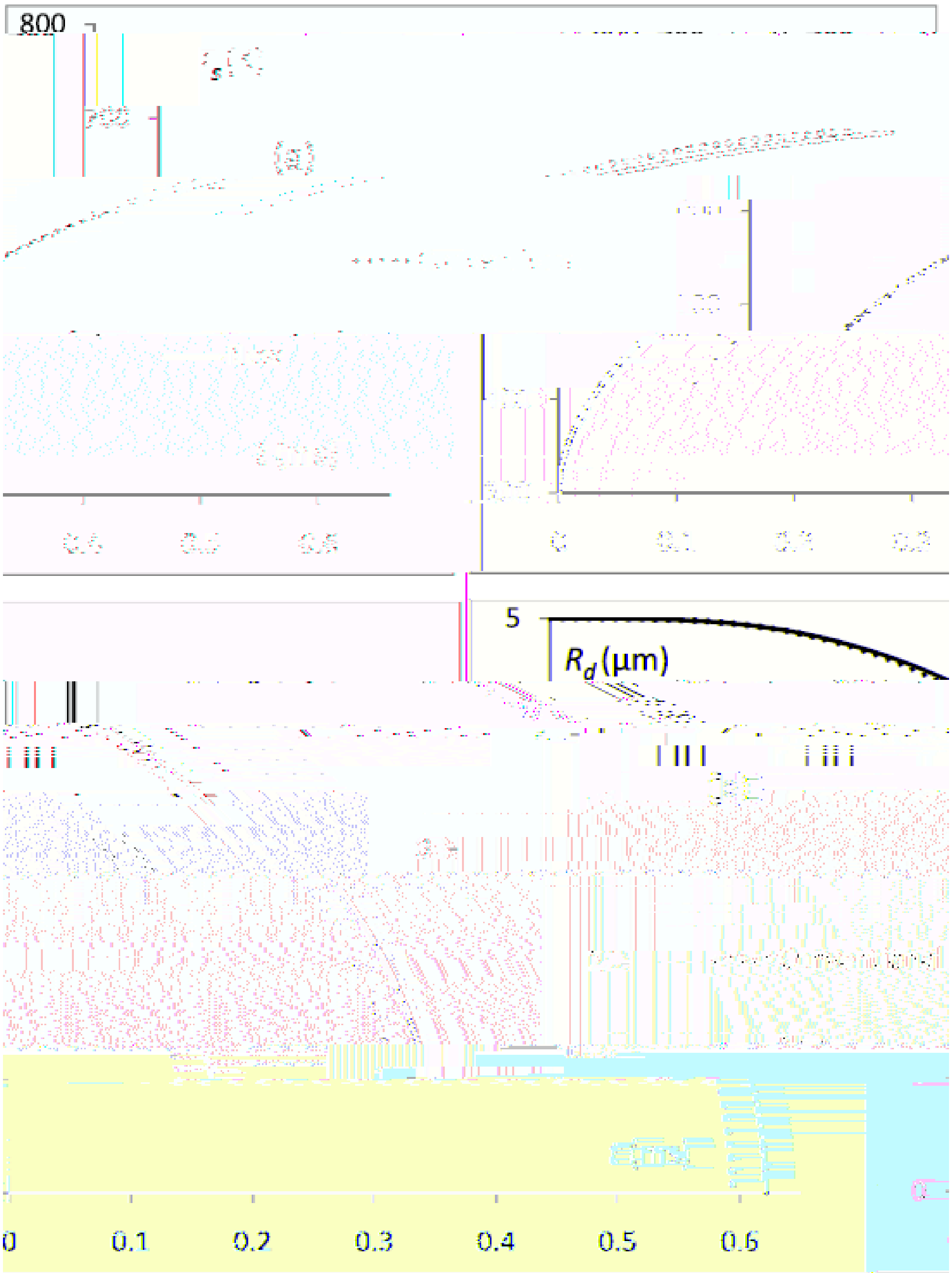

Figure 2.4: The plots of T_s versus time (a) and R_d versus time (b) for heated and evaporating droplets using the conventional (dotted), and new (solid) approaches for T_g = 1000 K and R_{d0} = 5 m.

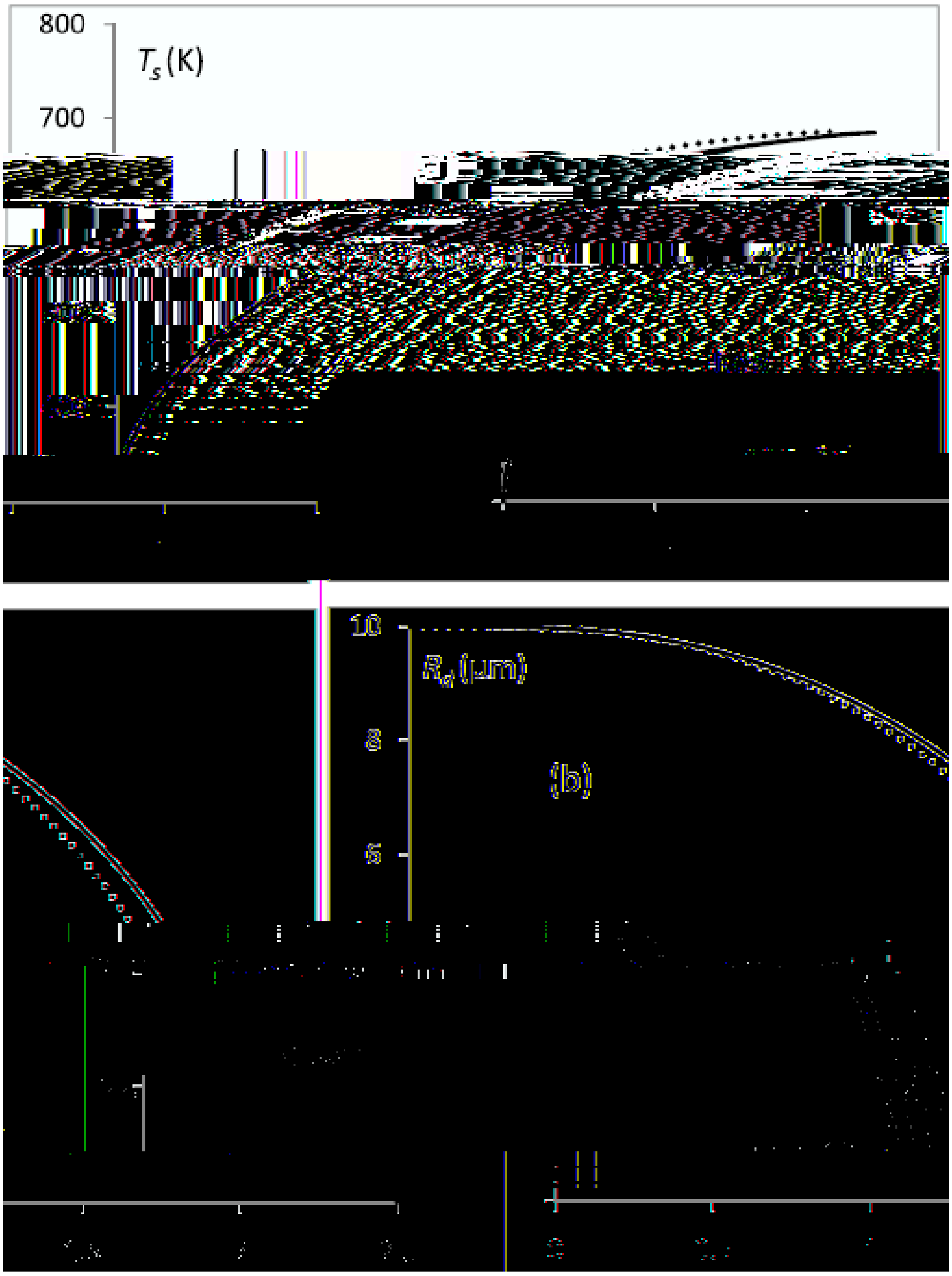

Figure 2.5: The same as Fig. 2.4 but for R_{d0} = 10 m.

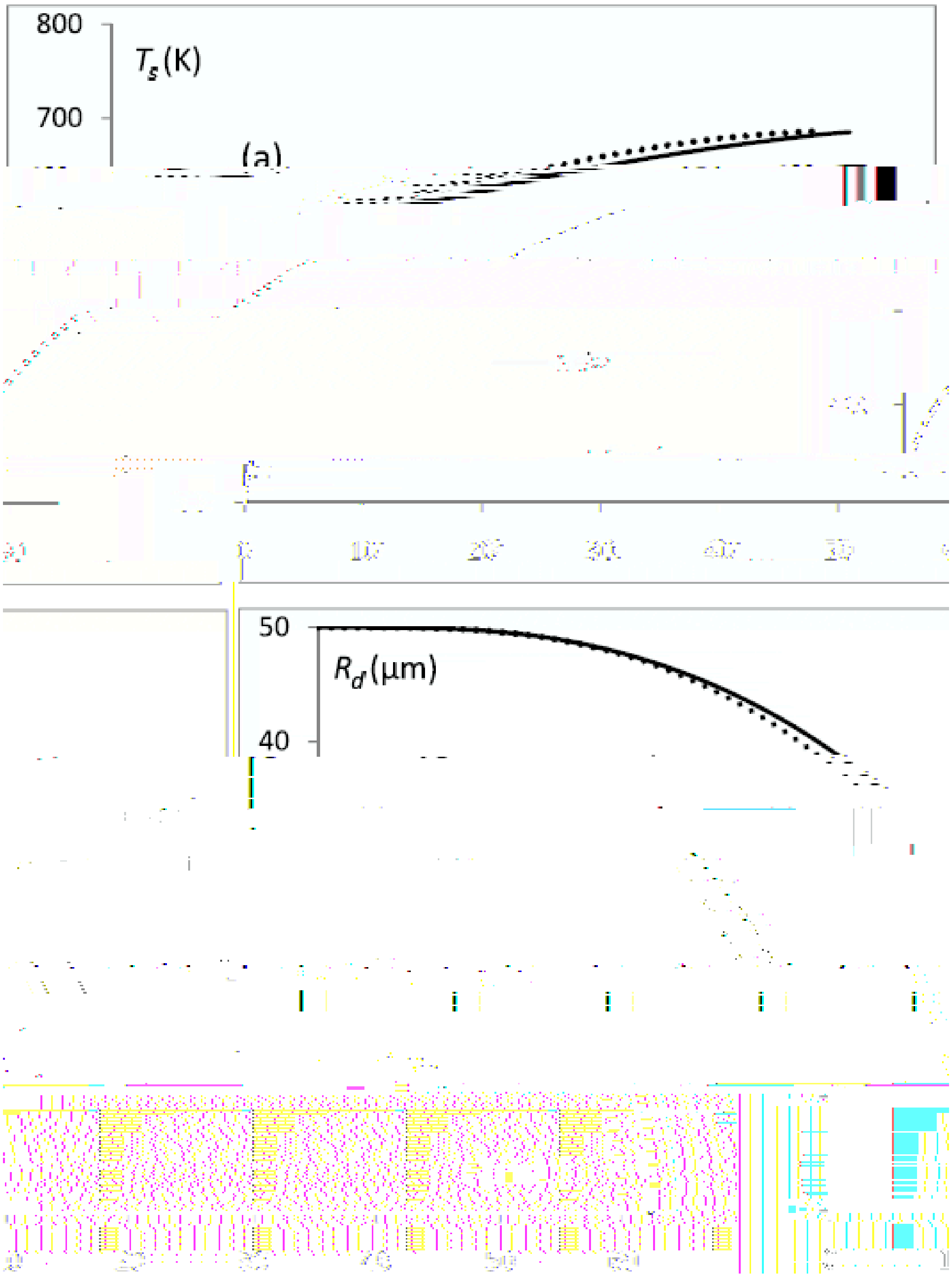

Figure 2.6: The same as Fig. 2.4 but for R_{d0} = 50 m.

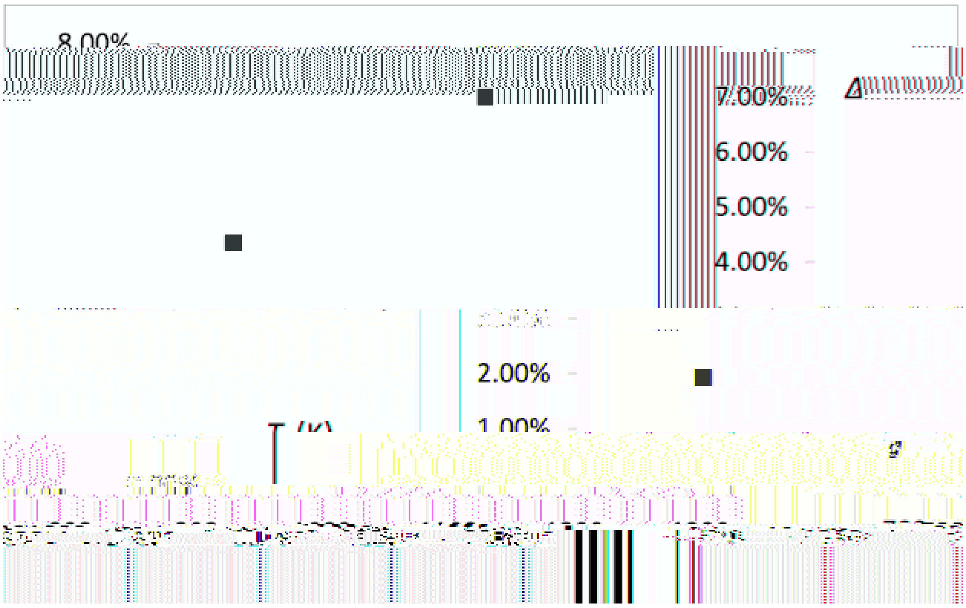
8.00%
7.00%
6.00%
5.00%
4.00%
2.00%
1.00%

To compare results obtained using different methods dimensionless variables are used: $R = \frac{R_d}{R_{d0}}$; $\quad {}_s = \frac{T_s \quad T_0}{T}$

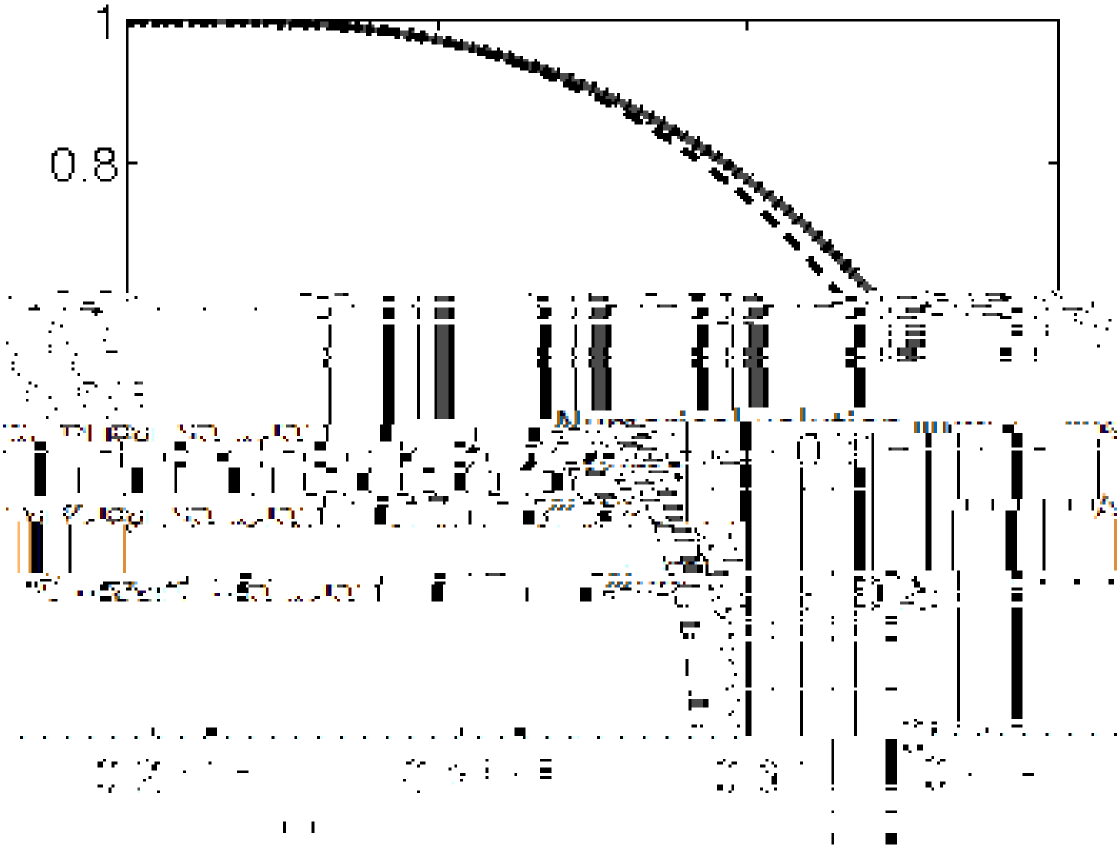

Figure 2.10: Comparison of R vs. t obtained using three di erent methods: the box scheme (solid); the method developed in this chapter (dotted); and the conventional method for which $R(t)$ is piecewise constant in time (dashed).

the result obtained, assuming that $R(t)$ is piecewise constant in time, and the results taking into account the changes of $R(t)$ during time steps. The results predicted by the numerical solution coincides within the accuracy of plotting with the one predicted by the model described in this chapter (as in the case shown in Fig. 2.9).

It is indicated in [23] that, for given values of T_0 and T_g, the maximum surface temperature reached is always the same, regardless of the initial droplet radius. Note that this maximal temperature (wet-bulb temperature) is asymptotically approached only in the case when the contribution of thermal radiation is ignored; when this contribution is taken into account, the droplet temperature reaches its maximal temperature, which is greater than the wet-bulb temperature, and then decreases, approaching the wet-bulb temperature from above [44]. Fortunately, for the case of negligible thermal radiation, we are able to investigate this further analytically, as shown in [23]. In brief, an analytical solution can be found as $t \to t_e$; and from this we

3.2 Solution for the case of arbitrary $R_d(t)$ but $T_{d0}(R) = \text{const}$

The analysis of this Chapter is based on the assumption that $T_{d0}(R) = T_{d0} = \text{const}$. In this case we can introduce the new variable $v = u \quad RT_{d0}$ and rearrange Equation (2.12) as:

$$\frac{\partial v}{\partial t} = \quad \frac{\partial^2 v}{\partial R^2} \tag{3.1}$$

for $t \in (0; t_e)$ and $R \in (0; R_d(t))$ with the boundary conditions

$$\left(\frac{\partial v}{\partial R} + H(t) v \right) \Bigg|_{R=R_d(t)} = \quad _0(t); \tag{3.2}$$

$$v|_{R=0} = 0 \tag{3.3}$$

for $t \in (0; t_e)$ and the initial condition

[illegible]

2) It satisfies Conditions (3.3) and (3.4);

3) It is continuous at $R \to R$

(cf. Equation (3.9)). Therefore, the integral in Equation (3.10) is de ned as an improper integral.

Note that $G_1(t; R = 0) = 0$.

Function $U(t; R)$ has the following properties [105, 130]:

1) It satisfies Equation (3.1) for $0 < t < t_e$ and $0 < R < \infty$;

2) It satisfies the boundary Condition (3.3) for $0 < t < t_e$;

3) It satisfies the initial condition

$$U(t; R)|_{t=+0} = \begin{cases} RT_{d0}(R) & \text{when } 0 \le R \le R_e \\ 0 & \text{when } R > R_e \end{cases} . \tag{3.15}$$

The latter relation follows from the property of the delta-function:

$$\lim_{\delta \to \infty} \frac{\delta}{\sqrt{\pi}} \exp(-\delta^2 x^2) = \delta(x). \tag{3.16}$$

We look for the solution to Equation (2.12) in the form:

$$u(t; R) = U(t; R) + v(t; R). \tag{3.17}$$

Having substituted Equation (3.17) into Equation (2.12) and boundary and initial conditions (2.13) – (2.15), we obtain problem (3.1) – (3.4) for $v(t; R)$ in which

$$\psi_0(t) = -\left[U'_R(t; R) + H(t)U(t; R) \right]_{R=}$$

Hence, we obtain an explicit expression for $_0(t)$ in the form:

$$_0(t) = \frac{1}{4\sqrt{\ }(\ t)^{3/2}} \int_0^{R_e} (\ T_{d0}(\ ))\ \Big\{ (R_d(t) \quad) \exp\left[\frac{(R_d(t) \quad)^2}{4\ t} \right]$$

$$(R_d(t) + \ ) \exp\left[\frac{(R_d(t) + \ )^2}{4\ t} \right] \Big\} d$$

$$\frac{H(t)}{2\sqrt{\ t}} \int_0^{R_e} (\ T_{d0}(\ )) \Big\{ \exp\left[\frac{(R_d(t) \quad)^2}{4\ t} \right] \quad \exp\left[\frac{(R_d(t) + \ )^2}{4\ t} \right] \Big\} d$$

$$+ M(t) R_d(t). \tag{3.21}$$

In the limit $t \to 0+$ the expression for $_0(t)$ is simplified to (see Appendix 5):

$$_0(0) = \quad (\ T_{do}(\ ))' \Big|_{=R_{d0}} + H(0) R_{d0} T_{d0}(R_{d0}) \ + \ (0). \tag{3.22}$$

Combining Equations (3.5) and (3.17) we can present the final solution to our problem in the form:

$$T(t;R) = \frac{1}{R} \Big[U(t;R) + \frac{\sqrt{\ }}{\quad}$$

3.4 Implementation of the new solutions into a numerical code

In the solutions presented in the last two sections it was assumed that $R_d(t)$ is

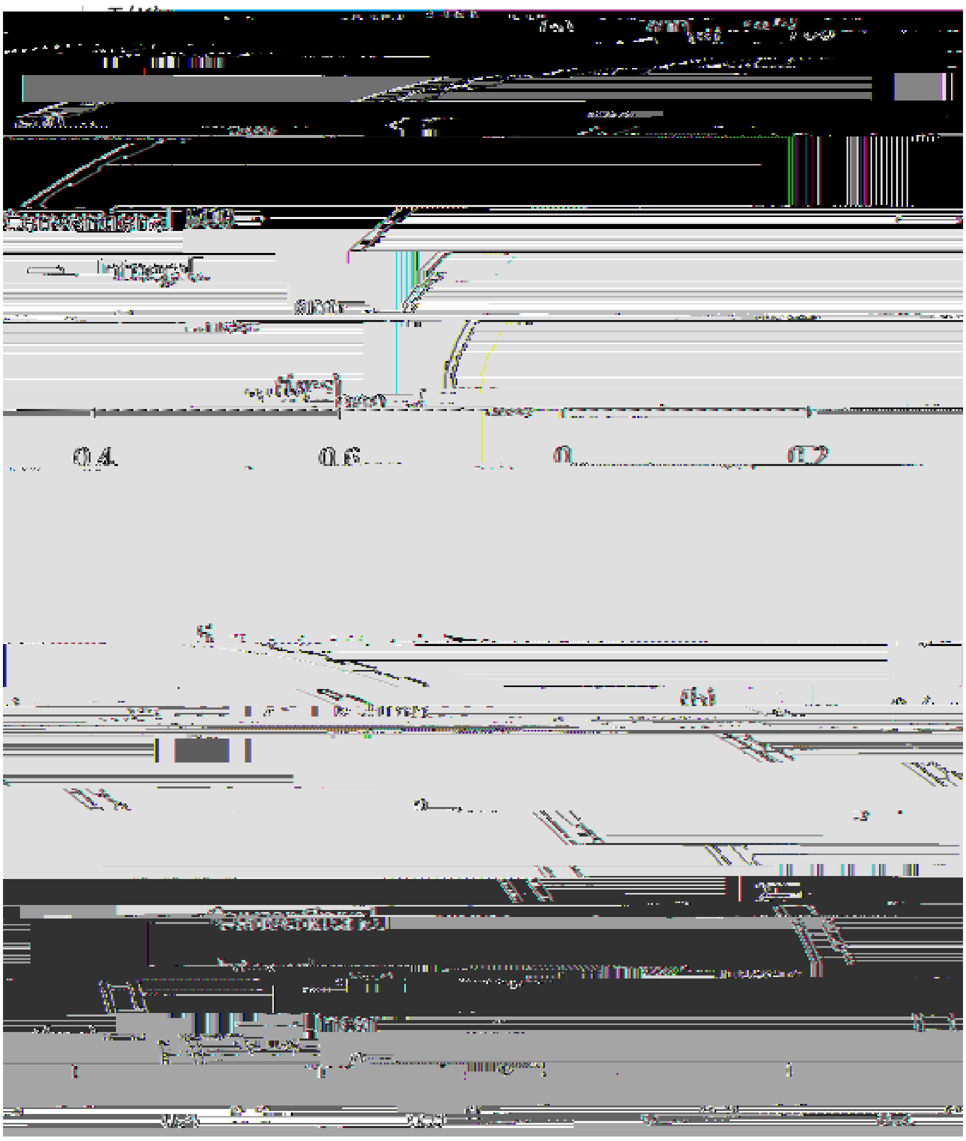

Figure 3.1: The plots of T_s versus time (a) and R_d versus time (b) using the conventional model (thick solid), integral model based on Equation (3.11) (dashed) and linear model (thin solid) for a stationary n-dodecane (M_f = 170 kg/kmole) droplet with an initial radius 5 m, evaporating in ambient air at a pressure of p = 30 atm = 3000 kPa and temperature 1000 K.

and linear solution (2.45) practically coincide, which suggests that both approaches are correct and valid. Both these solutions predict lower droplet temperatures and longer evaporation times in agreement with the results reported in previous Chapter. Note that deviations between the predictions of the integral and linear solutions were observed in the immediate vicinity of the time when the droplet completely evaporates.

There were obvious numerical problems when we approached this time due to the fact that the time derivative of R_d becomes infinitely large. In practice the extrapolation, based on the assumption that the second derivative of $R_d(t)$ is constant, was used for these times. This leads to small deviations between the predicted evaporation times. In the case shown in Fig. 3.1, the evaporation times predicted by the conventional model, linear solution, and integral solution were 0.595 ms, 0.622 ms and 0.628 ms respectively. That means that the difference between the evaporation times predicted by the linear and integral solutions was less than 1% and can be safely ignored in most practical applications (this error can be reduced further if required). The same comment applies to other cases considered below.

The effect of the choice of the number of iterations on the prediction of the integral solution is illustrated in Fig. 3.2 for the same case as shown in Fig. 3.1. This effect is shown only for the times when the deviation between the results predicted by the linear and integral solutions is maximal. For the first iteration, the time evolution of droplet radius is the same as predicted by the conventional model. The deviation of the corresponding droplet temperatures predicted by the integral and linear solutions appears to be quite noticeable. For the fifth iteration the droplet surface temperatures predicted by the integral and linear solutions practically coincide up to $t \leq 0.45$ ms. The corresponding plots of $R_d(t)$, predicted by the integral solution, turned out to be closer to those predicted by the linear solution than those predicted by the conventional model. The closeness between the plots predicted by the linear and integral solutions improved as the number of iterations increased. However, even for the 15th iteration the deviation between the results remains visible, although not important for practical applications (cf. Fig. 3.1). For higher iterations the results are practically indistinguishable from those predicted by the 15th iteration. Interestingly, odd iterations predicted smaller $R_d(t)$ and even iterations

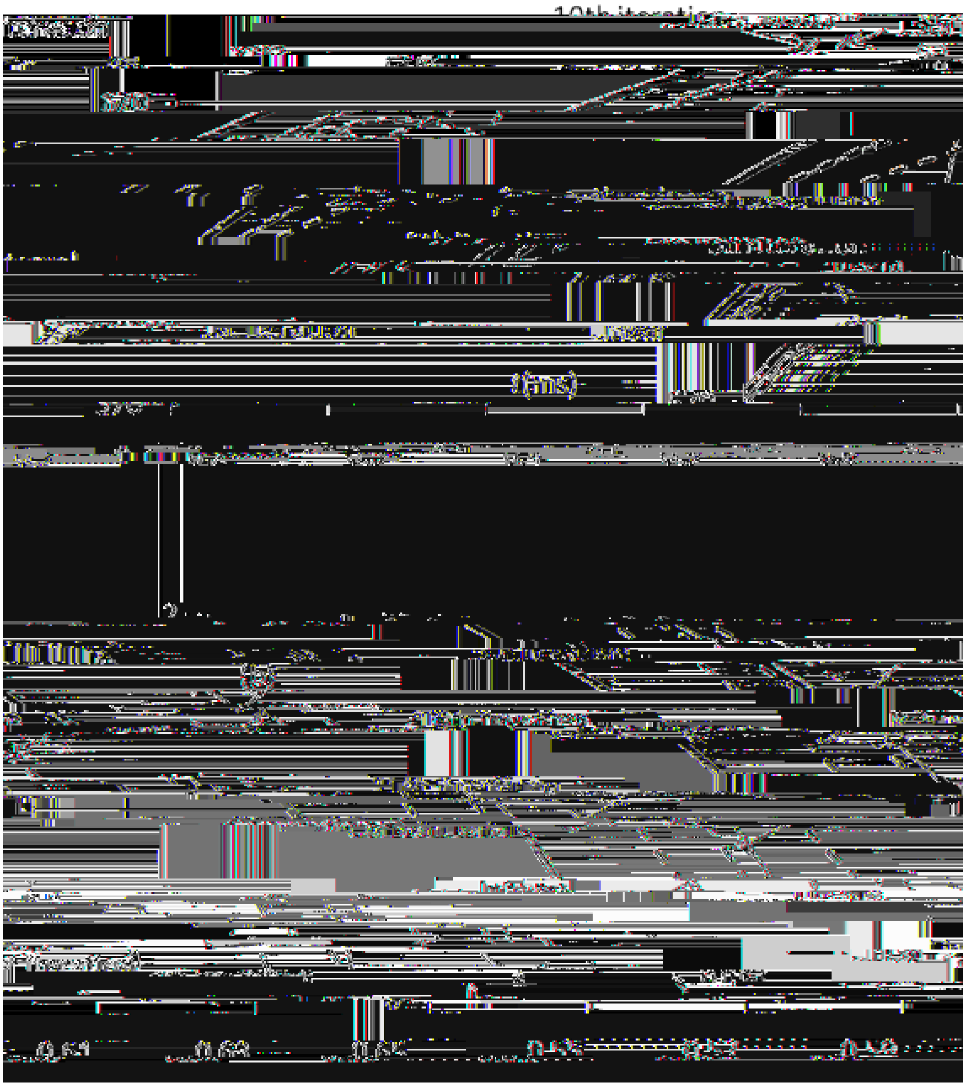

Figure 3.2: The same as Fig. 3.1 but for di erent numbers of iterations in the integral solution.

predicted larger $R_d(t)$ compared with those predicted by the linear solution. At the qualitative level this could be related to the fact that a faster evaporation rate, assumed for the rst iteration (conventional model), leads to a lower droplet surface temperature. At the second iteration, this lower droplet surface temperature leads to a slower evaporation rate etc.

As to the computational e ciency of the new integral model, we note that for a PC Xeon 3000 Hz (the calculations were processed on one kernel only) with 2357(23))-32B-2

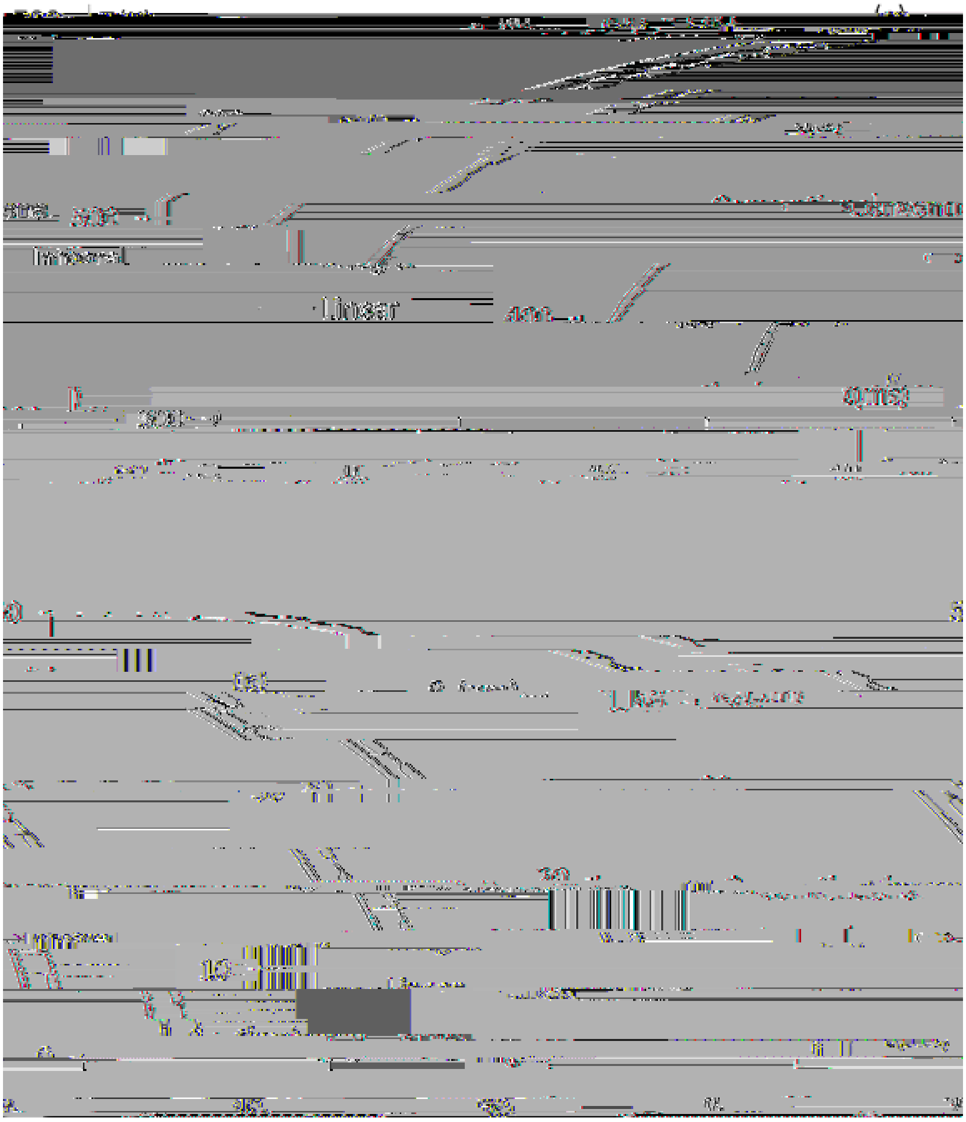

Figure 3.3: The same as Fig. 3.1 but for a droplet with initial radius 50 m.

computational uid dynamics (CFD) codes.

The results, similar to those shown in Fig. 3.1, but for droplets with initial radii 50 and 100 m are shown in Figs. 3.3 and 3.4 respectively. As can be seen from these gures, the plots of droplet surface temperatures and radii are largely una ected by

Figure 3.4: The same as Figs. 3.1 and 3.3 but for a droplet with initial radius 100 m.

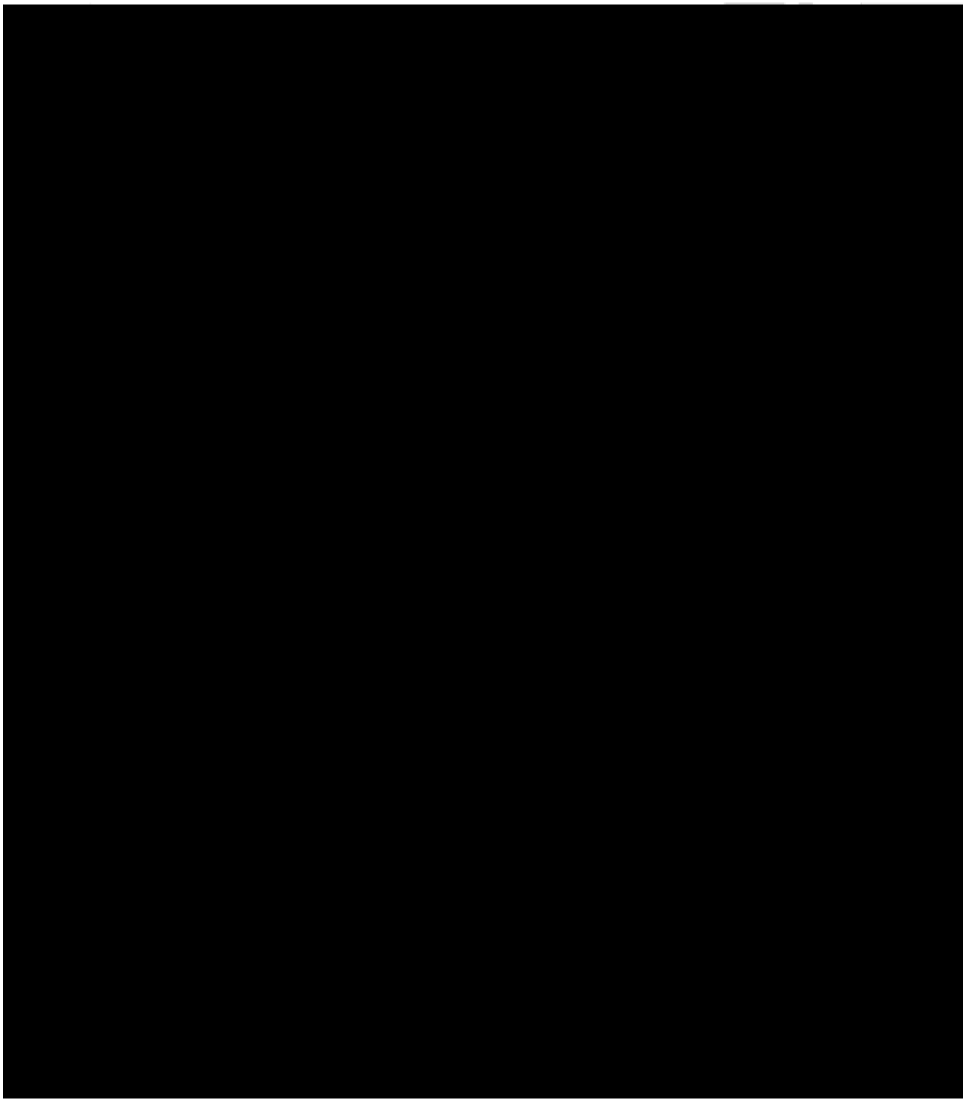

Figure 3.6: The same as Figs. 3.1 and 3.5 but for an ambient gas temperature equal to 1200 K.

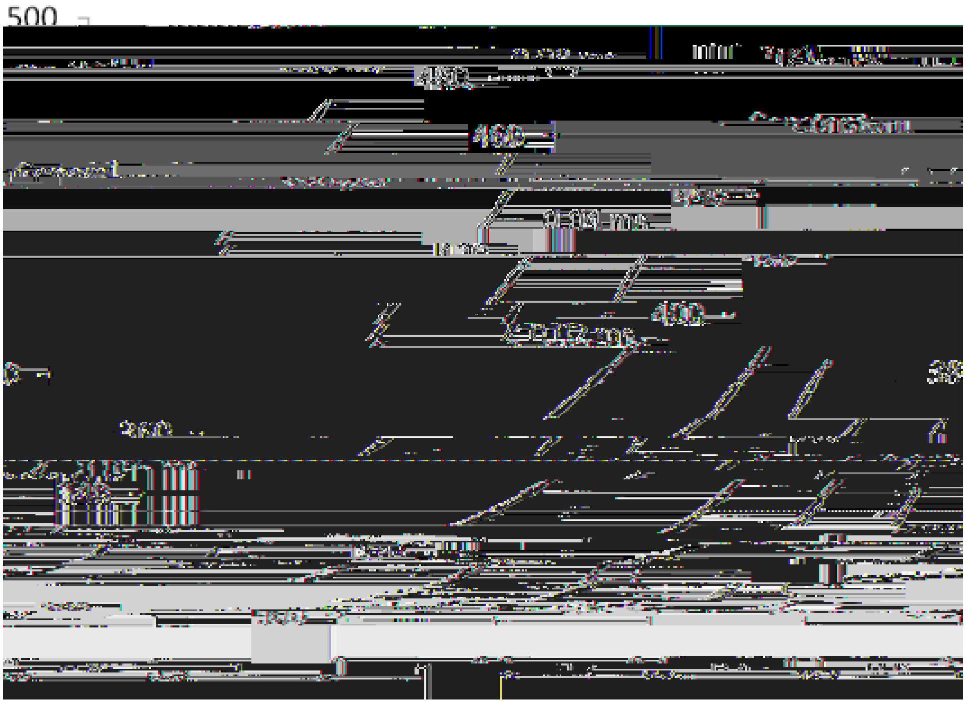

Figure 3.7: The plots of T versus $= R/R_d$ for a stationary n-dodecane ($M_f = 170$ kg/kmole) droplet with initial radius 5 m, evaporating in ambient airting

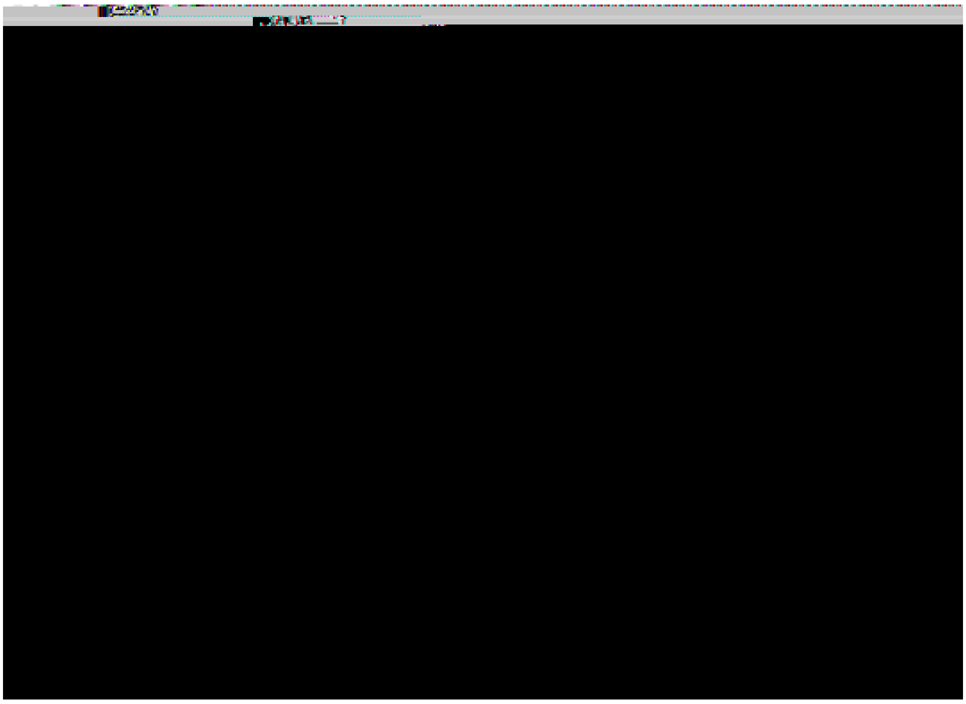

Figure 3.8: The same as Fig. 3.7 but for the general solution (Equation (3.23) applied to the case when the initial distribution of temperature inside the droplet is given by Equation (3.24)).

distribution of droplet temperature was approximated as

$$T_{d0}(R) = 300 + 10(R/R_{d0})^2 = 300 + 10(\;)^2; \qquad (3.24)$$

and the analysis was based on Equation (3.23).

Comparing the plots referring to both cases, shown in Fig. 3.8, one can see that these plots visibly converge with time. This can be related to the fact that increased droplet surface temperature in the general case leads to decreased convective heating of droplets. Hence the droplet surface temperature increases more slowly in the general case than in the case of constant initial temperature inside droplets.

We appreciate that the errors associated with the conventional assumption that the droplet radii remain constant during the time step can be comparable with or even larger than those associated with other effects, including uncertainties in gas temperature measurements, convection heat transfer coefficient approximations and effect of interactions between droplets in realistic sprays. The importance of the latter effect is discussed in [14, 38], but its analysis lies beyond the scope of this Chapter.

3.6 Conclusions of Chapter 3

Two new solutions to the heat conduction equation, describing transient heating of an evaporating droplet, are suggested, assuming that the time evolution of droplet radius $R_d(t)$ is known. The initial droplet temperature is assumed to be constant or allowed to change with the distance from the droplet centre. The results turned out to be the simplest in the first case and the main focus of our analysis is upon these. Since $R_d(t)$ depends on the time evolution of the droplet temperature, an iterative process is required. Firstly, the time evolution of $R_d(t)$ is obtained using the conventional approach, when it remains constant during the time step, but changes from one time step to another. The droplet surface temperature in this case is obtained from the analytical solution of the heat conduction equation inside the droplet. It is assumed that this droplet is heated by convection from the ambient gas, and its radius remains constant during the time step. Then these values of $R_d(t)$ are used in the new solutions to obtain updated values of time evolution of the distribution of temperatures inside the droplet and on its surface. These new values of droplet temperature are used to update the function $R_d(t)$. This process continues until convergence is achieved, which typically takes place after about 15 iterations. The results of the calculations of droplet surface temperature, using this approach, are compared with the results obtained using the previously suggested approach when the droplet radius was assumed to be a linear function of time during individual time steps for typical Diesel engine-like conditions. For sufficiently small time steps the time evolutions of droplet surface temperatures and radii, predicted by both approaches coincide. This suggests that both approaches are correct and valid. Similarly to the case when droplet radius is assumed to be a linear function of time during the time step, the new solution predicts lower droplet temperatures and slower evaporation when the effects of the reduction of R_d are taken into account.

It is shown that in the case of constant droplet initial temperature, models both taking and not taking into account the changes in initial droplet temperature with the distance from the droplet centre, predict the same results. This suggests that both models are likely to be correct. It is shown that the temperatures predicted by the models based on the assumption of constant initial droplet temperature, and the one taking into account the increase in this temperature with the distance from the droplet centre, tend to converge with time.

Chapter 4

New solutions to the species di usion equation inside droplets in the presence of the moving boundary

4.1 Introduction of Chapter 4

The species di usion equation, describing the dynamics of multi-component systems, its analysis and applications, has been widely discussed in the literature [53]. One of

and the initial condition $Y_{li}(t = 0) = Y_{li0}(R)$, where $Y_{lis} = Y_{lis}(t)$ are liquid components' mass fractions at the droplet's surface,

$$_m = \frac{j\underline{m}_d j}{4 \quad {}_l R_d^2};\tag{4.3}$$

$_i$ is the evaporation rate of species.

Note that 0

The latter velocity was calculated as [44]:

$$U_s = \quad 1$$

by correcting the expression for $\mathrm{Sh}_{\mathrm{iso}}$ (see [38, 49] for details). This e ect is not taken into account in our analysis.

Note that Equation (4.10) is valid for arbitrary Lewes numbers, while the equation for $\underline{m}_d$ used in Chapters 2 and 3 is valid only for Lewes numbers equal to 1.

To calculate the species mass evaporation rate $\underline{m}_i$ and the values of the evaporation rate of species $_i$

These allow us to rewrite Equation (4.1), the corresponding initial condition and boundary condition (4.2) as:

$$R_d^2(t) W_t'(t;\ ) = D_l W''(t;\ ); \tag{4.15}$$

where t 0,

$$W(t;\ )|_{t=0} = W_0(\ ) \quad R_{d0}^{3/2}\ Y_{li0}(\ R_{d0}) \exp\left[\frac{R_d'(0)R_{d0}}{4D_l}\ {}^2\right]; \tag{4.16}$$

$$W(t;\ )|_{\ =0} = 0; \tag{4.17}$$

$$\begin{aligned} &\left[W'(t;\ ) + H_0(t)W(t;\ )\right]_{\ =1} \\ &= \ {}_0(t) \qquad \frac{\ {}_m\ {}_i\,(R_d(t))^{5/2}}{D_l} \exp\left[\frac{R_d'(t)R_d(t)}{4D_l}\right]; \end{aligned} \tag{4.18}$$

where:

$$H_0(t) = \quad \frac{\ {}_m}{D_l} R_d(t) \quad 1 \quad \frac{R_d'(t)R_d(t)}{2D_l}.$$

Condition (4.17) is an additional boundary condition, which follows from the requirement that $Y_{li}(t;R)$ is a twice continuously differentiable function. When deriving (4.15) we took into account that $\mathrm{d}^2R_d/\mathrm{d}t^2 = 0$.

Further simplification of Equation (4.15) and the corresponding initial and boundary conditions is possible when we apply this equation to a short time step. In this

The initial and boundary conditions for Equation (4.21) can be presented as:

$$V(t;\ )|_{t=0} = W_0(\ ) \quad \frac{_0(0)}{1 + h_0}\ ;$$

$$V(t;\ )|_{\ =0} = 0; \qquad \left[V'(t;\ ) + h_0 V(t;\ ) \right]_{\ =1} = 0.$$

As in Chapter 2, we look for the solution of Equation (4.21) in the form:

$$V(t;\ ) = \sum_{n=0}^{\infty} \ _n(t) v_n(\ ); \tag{4.22}$$

where functions $v_n(\ )$ form the full set of non-trivial solutions to the equation:

$$\frac{d^2 v}{d\ ^2} + pv = 0; \quad 0 \qquad 1; \tag{4.23}$$

subject to boundary conditions:

$$v|_{\ =0} = \left(\frac{dv}{d\ } + h_0 v \right)_{\ =1} = 0. \tag{4.24}$$

For $p = 0$, Equation (4.23) has no non-trivial solutions, satisfying the boundary conditions (4.24). For $p \qquad ^2 < 0$, this equation has the solution:

$$v_0(\ ) = \sinh(\ _0\ ); \tag{4.25}$$

where $\ _0$ is the solution to the equation

$$\tanh \quad = \quad \frac{}{h_0}. \tag{4.26}$$

The latter equation has three solutions (positive, negative and zero) remembering that $h_0 < \ 1$. We are interested in the positive solution to this equation only [19].

Note that this solution does not exist in the case of the heat conduction equation, when h_0 is greater than $\ 1$ (see Chapter 2).

For $p \qquad ^2 > 0$, Equation (4.23) has the solutions:

$$v_n(\ ) = \sin(\ _n\ ) \tag{4.27}$$

for $n \quad 1$, where $\ _n$ are the solutions to the equation

$$\tan \quad = \quad \frac{}{h_0}. \tag{4.28}$$

As in the case $p < 0$ we disregard the solutions to this equation corresponding to zero and negative . A countable set of positive solutions to this equation (positive eigenvalues) $\ _n$ are arranged in ascending order:

$$0 < \ _1 < \ _2 < \ _3 < \ldots.$$

It can be shown that functions $v_n(\ )$, $n \quad 0$ are orthogonal for $0 \qquad 1$ (see Chapter 2).

The completeness of the set of functions $v_n(\ )$ for $n \quad 0$ has been tested. Namely, we considered di erent functions not belonging to this set, and found that Fourier expansions of these functions on the set of $f v_n(\ ) g^{1}_{n=0}$ coincide with the functions themselves. If the set of functions is not complete, then a Fourier expansion of

The general solution to the homogeneous equation:

$$R_d^2(t)\frac{\mathrm{d}\ \ _n(t)}{\mathrm{d}t} + (\ \ 1)^{\ \ n;0}\ \ _n(t)D_l\ \ ^2_n = 0 \tag{4.35}$$

can be presented as:

$$\ln(\ \ _n(t)/\ \ _n(0)) = \ \ (\ \ 1)^{\ \ n;0}D_l\ \ ^2_n\int_0^t \frac{\mathrm{d}t}{R_d^2(t)}: \tag{4.36}$$

Assuming that $R_d(t)$ is a linear function of t given by Equation (2.8), Solution (4.36) can be presented in a more explicit form:

$$_n(t) = \ \ _n(0)\exp\left[\frac{(\ \ 1)^{\ \ n;0}D_l\ \ ^2_n}{R_{d0}^2}\ \ \frac{1}{1+\ \ t}\ \ 1\right]: \tag{4.37}$$

One can see that the following function:

n (^2_d he)-326(homogeneous)-327(equatio)1(n:)]TJ/F22 9-1

Remembering that Solution (4.41) is applied to a very short time step, changes of $\mu_0(\tau)$ in the integrand before the exponential term can be ignored. This allows us to simplify (4.41) to (see Appendix 6):

$$\Theta_n(t) = [q_n + f_n \mu_0(0)] \exp\left[-(-1)^{\delta_{n;0}} \frac{D_l \lambda_n^2 t}{R_{d0} R_d(t)}\right] + f_n \mu_0(t) - f_n \mu_0(0). \qquad (4.42)$$

Note that $\Theta_n(t)$ in the form (4.40) satisfies Equation (4.33), while $\Theta_n(t)$ in the form (4.42) does not satisfy it. This is related to the fact that Equation (4.33) was derived under the assumption that Series (4.22), after being substituted into Equation (4.21), can be differentiated term by term (derivative of the series is equal to the series of derivatives). This assumption is valid when $\Theta_n(t)$ is taken in the form (4.40), but it is not valid when $\Theta_n(t)$ is taken in the form (4.42), as:

$$\mu_0(t) \frac{\mathrm{d}^2}{\mathrm{d}\zeta^2} \left(\sum_{n=0}^{\infty} f_n v_n \right) \neq \mu_0(t) \sum_{n=0}^{\infty} f_n \frac{\mathrm{d}^2 v_n}{\mathrm{d}\zeta^2}$$

(the series on the right hand side of this formula diverges). Note that Series (4.22) satisfies Equation (4.21) regardless of whether $\Theta_n(t)$ is taken in the form (4.40) or in the form (4.42).

Remembering (4.30) and (4.42), Equation (4.22) can be rewritten as:

$$V(t;\zeta) = \sum_{n=0}^{\infty} \Theta_n(t) v_n(\zeta) - \frac{\mu_0(t)}{1+h_0} \frac{R}{R_d(t)} + \frac{\mu_0(0)}{1+h_0} \frac{R}{R_d(t)}, \qquad (4.43)$$

where

$$\Theta_n(t) = [q_n + f_n \mu_0(0)] \exp\left[-(-1)^{\delta_{n;0}} \frac{D_l \lambda_n^2 t}{R_{d0} R_d(t)}\right]. \qquad (4.44)$$

The final equation for mass fraction inside the droplet can be presented as:

$$Y_{li}(R) = \frac{1}{R\sqrt{R_d(t)}} \exp\left[-\frac{R_{d0} R^2}{4 D_l R_d(t)}\right] \left[\sum_{n=1}^{\infty} \Theta_n(t) \sin\left(\lambda_n \frac{R}{R_d(t)}\right) + \mu_0(t) \sinh\left(\lambda_0 \frac{R}{R_d(t)}\right) + \frac{\mu_0(0)}{1+h_0} \frac{R}{R_d(t)}\right], \qquad (4.45)$$

where Θ_n are given by Equations (4.44).

Having substituted (4.44) into (4.45) we can rearrange the latter equation for the short time step to

$$Y_{li}(R) = \frac{\alpha_m \epsilon_i \exp\left[\frac{R_{d0}}{4D_l} \frac{R_{d0} R_d(t) - R^2}{R_d(t)}\right]}{\alpha_m + \frac{R_{d0}}{2}} \frac{R_{d0}^{5/2}}{R_d^{5/2}(t)} + \frac{1}{R\sqrt{R_d(t)}} \exp\left[-\frac{R_{d0} R^2}{4 D_l R_d(t)}\right]$$
$$\left[\sum_{n=1}^{\infty} [q_n + f_n \mu_0(0)] \exp\left[-\frac{D_l \lambda_n^2 t}{R_{d0} R_d(t)}\right] \sin\left(\lambda_n \frac{R}{R_d(t)}\right) + \right.$$

$$[q_0 + f_0\,\psi_0(0)]\exp\left[-\frac{D_l\lambda_0^2 t}{R_{d0}R_d(t)}\right]\sinh\left(\lambda_0\frac{R}{R_d(t)}\right)\Bigg] : \tag{4.46}$$

When $\alpha = 0$ but $\lambda_m \neq 0$ during the time step, Equation (4.46) can be further simplified to

$$Y_{li}(R) = \theta_i + \frac{1}{R\sqrt{R_d(t)}}\Bigg[\sum_{n=1}^{\infty}[q_n + f_n\,\psi_n(0)]\exp\left[-\frac{D_l\lambda_n^2 t}{R_{d0}R_d(t)}\right]\sin\left(\lambda_n\frac{R}{R_d(t)}\right) +$$

$$[q_0 + f_0\,\psi_0(0)]\exp\left[\frac{D_l\lambda_0^2 t}{R_{d0}R_d(t)}\right]\sinh\left(\lambda_0\frac{R}{R_d(t)}\right)\Bigg] : \tag{4.47}$$

This equation is identical to Equation (13) of [38]. Note that in [38] and [50] the norm of v_n ($||v_n||^2$) is dimensional. The ratio of $||v_n||^2$ used in [38, 50] and in this Chapter is equal to R_{d0}.

Let us now relax our assumption that $H_0(t) \equiv h_0 = \text{const}$ and assume that:

$$H_0(t) = h_0 + h_1(t); \tag{4.48}$$

where $h_0 = \text{const} < -1$. In view of (4.48) we can rewrite the boundary condition at $\mu = 1$ for Equation (4.15) in the form:

$$\left[W'(t;\mu) + h_0 W(t;\mu)\right]_{\mu=1} = \Phi_0(t) - h_1(t)W(t;1) \equiv \hat{\Phi}_0(t): \tag{4.49}$$

Assuming that $\hat{\Phi}_0(t)$ is known, we can formally use the previously obtained solutions (4.20) and (4.22) to present the solution to Problem (4.15)–(4.18) in the form:

$$W(t;\mu) = \frac{\hat{\Phi}_0(t)}{1+h_0} + V(t;\mu) = \sum_{n=0}^{\infty} v_n(\mu)\,q_n\exp\left[-(-1)^{\delta_{n;0}}\frac{D_l\lambda_n^2 t}{R_{d0}R_d(t)}\right]$$

$$-\sum_{n=0}^{\infty} v_n(\mu)(-1)^{\delta_{n;0}} f_n D_l\lambda_n^2$$

$$\int_0^t \frac{\hat{\Phi}_0(\tau)}{R_d^2(\tau)}\exp\left[-(-1)^{\delta_{n;0}}\frac{D_l\lambda_n^2}{R_{d0}}\left(\frac{1}{R_d(t)} - \frac{1}{R_d(\tau)}\right)\right]d\tau; \tag{4.50}$$

where Expression (4.41) for $\psi_n(t)$ has been used.

In contrast to the previous case of $H_0(t) = \text{const}$, Equation (4.50) does not give us an explicit solution for $W(t;\mu)$ since $\hat{\Phi}_0(t)$ depends on $W(t;1)$.

Equation (4.50) can be presented in a more compact form:

$$W(t;\mu) = V(t;\mu) - \int_0^t \hat{\Phi}_0(\tau)\,G(t;\mu;\tau)\,d\tau; \tag{4.51}$$

where

$$V(t;\quad) = \sum_{n=0}^{\infty} v_n(\quad) q_n \exp\left[\quad (\quad 1)^{n;0}\right.$$

[50]. Since the main focus of this Chapter is on the analysis of the new physical e ects produced by the droplet? moving boundary, the optimisation of the algorithm is beyond its scope (cf. the analysis of accuracy and CPU e ciency of the related algorithm, not taking into account the e ects of the moving boundary, described in Section 7 of [50]). Note that the speed of convergence of the algorithm turned out to be very high. Even calculations based on 100 time steps led to almost the same results as those based on 10^5 time steps. In the case of 100 time steps the CPU time was less than 5 sec. Calculations were performed on a 3 GHz CPU, 2 GB RAM work station.

4.4 Application to bi-component droplets

4.4.1 E ect of species di usion

In this section, Solution (4.47) is applied to the analysis of bi-component droplet heating and evaporation in an environment close to the one described in [38]. We

Figure 4.1: The plots of ethanol mass fraction Y_{eth} versus $\zeta = R/R_d$, as predicted by the conventional model (dashed) and the new model, taking into account the effect of the moving boundary (solid), for times 0.001 s, 0.01 s and 0.03 s. We consider an initial 50% ethanol – 50% acetone mixture and droplets with initial diameter equal to 142.7 μm.

shown in Fig. 4.1. As expected, both models predict the increase of Y_{eth} with increasing ζ and time. This is related to higher volatility of acetone in the ethanol/acetone mixture. As one can see from Fig. 4.1, at times less than 0.001 s the predictions of the conventional and the new models are practically indistinguishable. At later times, however, the new model always predicts lower values of Y_{eth} compared with the conventional model. In fact the effect of the moving boundary on the distribution of species looks stronger than a similar effect on the distribution of temperature inside droplets as reported in Chapter 2.

The plots of Y_{eth} at the droplet surface ($Y_{\mathrm{eth}}(\zeta = 1)$) versus time, predicted by the conventional model, and the new model, taking into account the effect of the moving boundary, are shown in Fig. 4.2. As one can see from this figure, both models predict the increase of $Y_{\mathrm{eth}}($

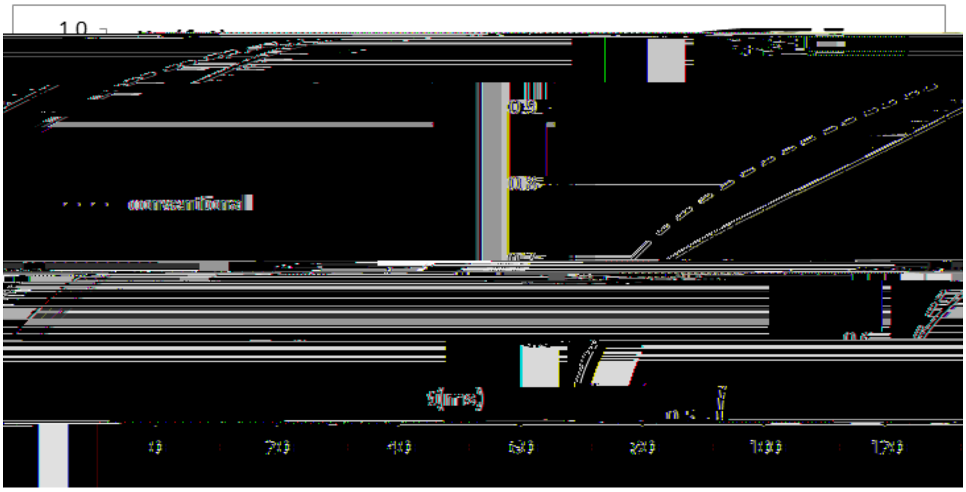

Figure 4.2: The plots of Y_{eth}(= 1) versus time, as predicted by the conventional model (dashed) and the new model, taking into account the e ect of the moving boundary (solid).

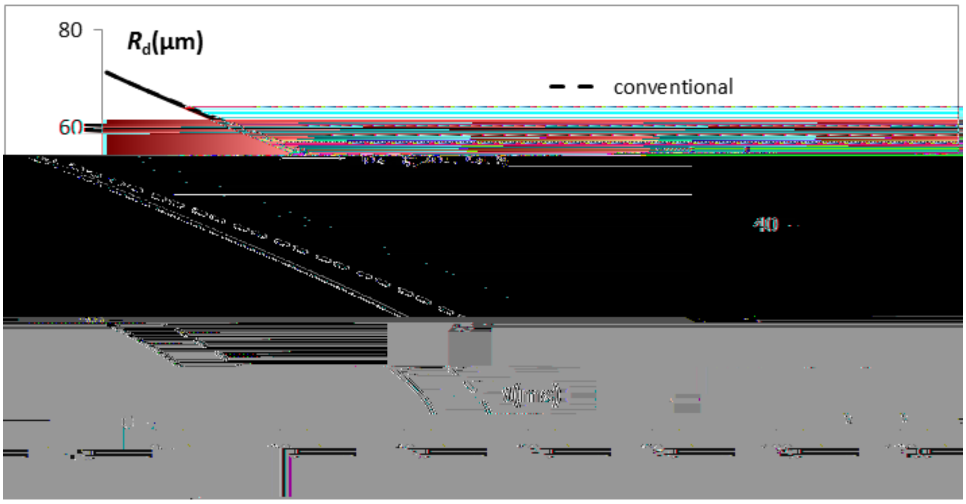

Figure 4.3: The plots of droplet radius R_d versus time, as predicted by the conventional model (dashed) and the new model, taking into account the e ect of the moving boundary (solid).

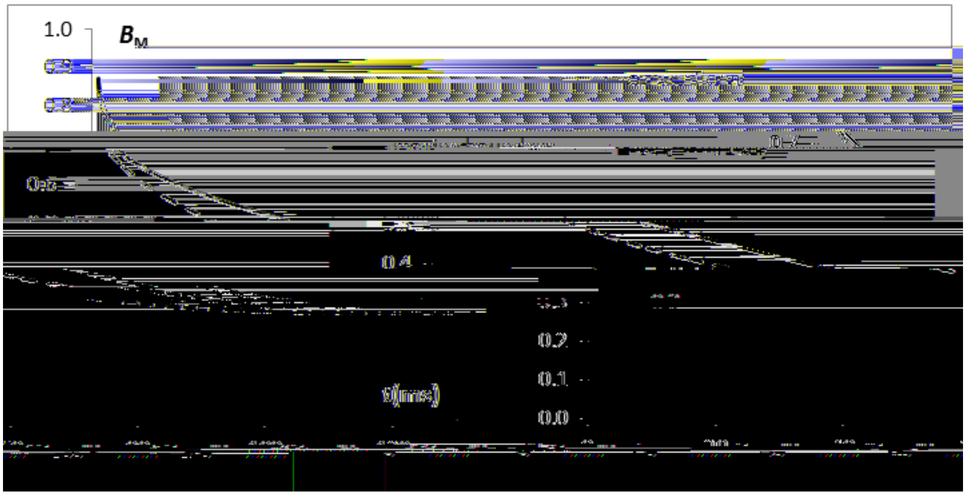

Figure 4.4: The plots of Spalding mass transfer number B_M versus time, as predicted by the conventional model (dashed) and the new model, taking into account the effect of the moving boundary (solid).

model, and the new model, taking into account the effects of the moving boundary, are shown in Fig. 4.3. As one can see from this figure, taking into account the effect of the moving boundary leads to the acceleration of droplet evaporation compared with the prediction of the conventional model. This effect is opposite to the one reported earlier for the effect of the moving boundary on the thermal conductivity inside droplets. In the latter case, the effect of the moving boundary led to slowing down of droplet evaporation. The physical background to the effect shown in Fig. 4.3 is that the new model predicts higher mass fraction of acetone at the surface of the droplet, as shown in Fig. 4.2, which evaporates faster than ethanol.

Note that for mono-component droplets at fixed temperature we would expect that the d^2 law should be valid. This is obviously not the case shown in Fig. 4.3. The reason for this is that the evaporation of multi-component droplets leads to changes in the Spalding mass transfer number B_M due to the changes in vapour composition near the droplet's surface. The plots of B_M versus time, predicted by the conventional model, and the new model, taking into account the effects of the moving boundary, are shown in Fig. 4.4. As can be seen from this figure, both models predict the decrease in B_M with time except at the final stage of droplet evaporation, when the droplet becomes mono-component, consisting only of ethanol. The new model predicts larger B_M compared with the conventional model. Note that except

shown to be close to a linear function. The relevant approximations of the experimental results are summarised in Table 4.1 (reproduced from [38]).

Substance	Droplet temp.	Diameter	Gas temp.	Dist. parameter
100% acetone	35.1 C	143.4 m	21.5 C	7.7
100% ethanol	38.0 C	140.8 m	22.0 C	7.1
25% ethanol + 75% acetone	32.5 C	133.8 m	21.1 C	8.7
50% ethanol + 50% acetone	37.5 C	142.7 m	20.8 C	7.53
75% ethanol + 25% acetone	38.6 C	137.1 m	21.6 C	7.53

Table 4.2: The measured initial values of droplet temperature, diameter, ambient gas temperature and distance parameter for the same cases as in Table 4.1.

The measured initial values of droplet temperature, diameter, ambient gas temperature and distance parameter C (ratio of the distance between droplets to their diameters) for the same cases as in Table 4.1 are shown in Table 4.2. Gas temperature was constant during the measurements. The changes in C from the previous to the current time step were taken into account based on the following equation:

$$C_{\mathrm{new}} = C_{\mathrm{old}} \frac{U_{\mathrm{drop,\,new}}}{U_{\mathrm{drop,\,old}}} \frac{R_{d,\,\mathrm{old}}}{R_{d,\,\mathrm{new}}}, \tag{4.57}$$

where subscripts $_{\mathrm{new}}$ and $_{\mathrm{old}}$ refer to the values of variables at the previous time step and one time step behind respectively. In this case the values of $R_{d,\,\mathrm{old}}$ and $R_{d,\,\mathrm{new}}$ are known at the current time step.

The plots of time evolutions of the temperatures at the centre and the surface of the droplets and the average droplet temperatures, predicted by the models not taking into account the effect of the moving boundary and taking into account this effect for both temperature and species diffusion for the 25% ethanol – 75% acetone and 50% ethanol – 50% acetone mixture droplets, are shown in Fig. 4.5. As can be seen from this figure, the effect of the moving boundary on the predicted temperatures can be safely ignored in the analysis of experimental data described earlier. The same conclusion can be drawn for the case of the 75% ethanol – 25% acetone mixture droplets (figure is not shown).

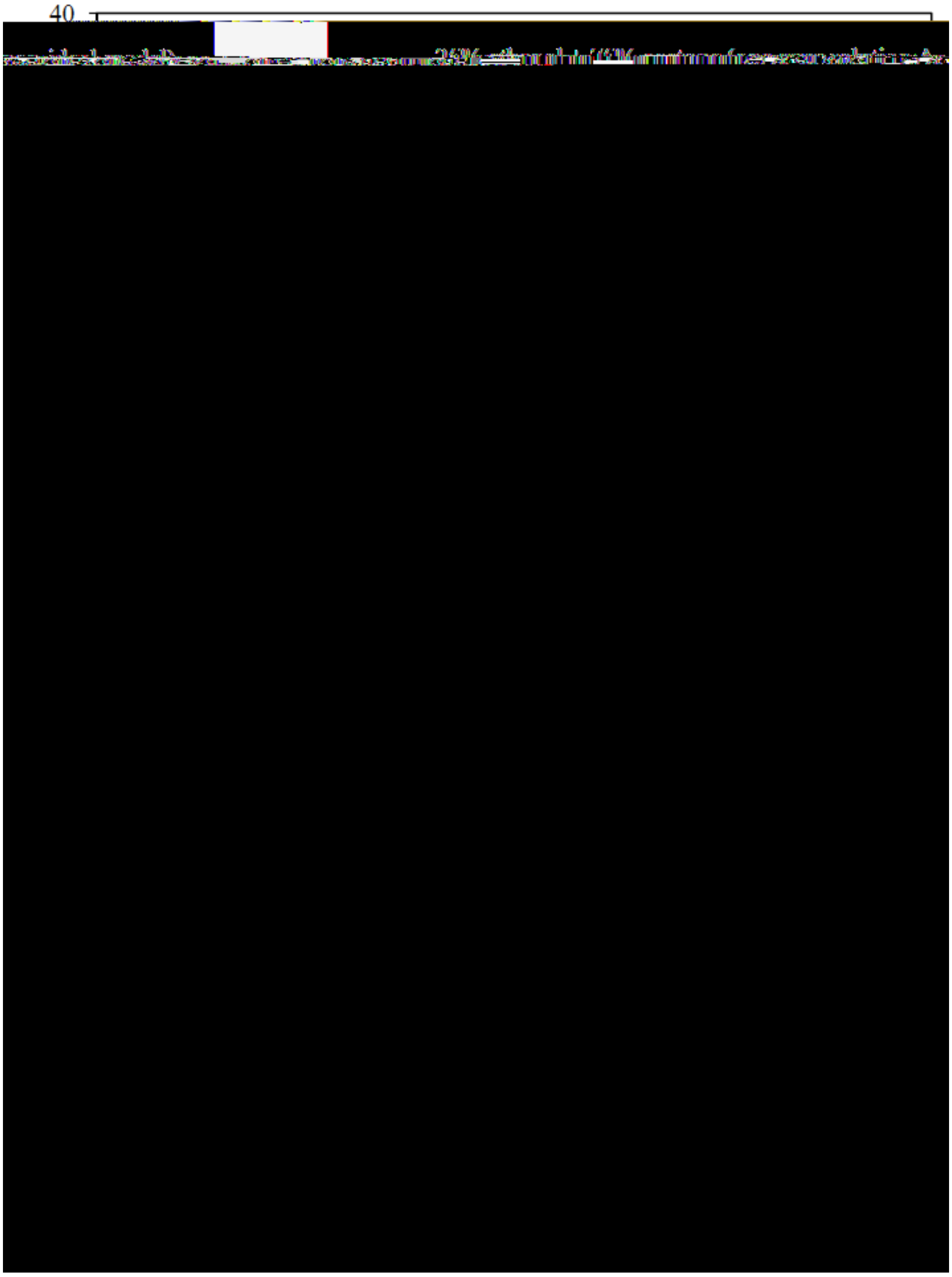

Figure 4.5: The time evolution of droplet surface, average and centre temperatures (T_s, T_{av} and T_c), predicted by the one-way Solution A for the non-ideal model, taking and not taking into account the e ects of the moving boundary during individual time steps (moving and stationary boundaries) on the solutions to both heat transfer and species di usion equations for the 25% ethanol { 75% acetone mixture droplets with the values of the initial parameters, droplet velocity and gas temperature given in Tables 4.1 and 4.2 (a); the same as (a) but for the 50% ethanol { 50% acetone mixture droplets (b).

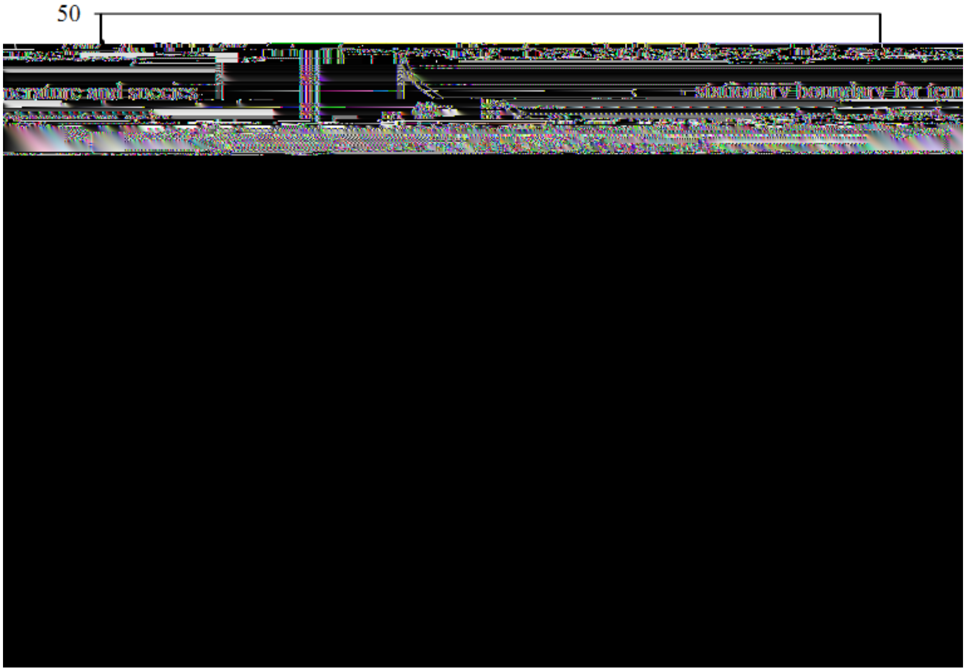

Figure 4.6: The time evolution of droplet surface temperatures (T_s) and radius (R_d), predicted by the one-way Solution A for the non-ideal model, taking and not taking into account the effects of the moving boundary during individual time steps on the solutions to the heat transfer equation only, species diffusion equation only and both heat transfer and species diffusion equations for the 50% ethanol – 50% acetone mixture droplets with the values of the initial parameters, and gas temperature given in Table 4.2, assuming that the droplet velocity is constant and equal to 12.71 m/s.

In Fig. 4.5 a hypothetical case is shown when the 50% ethanol – 50% acetone mixture droplets are cooled down or heated and evaporated until complete evaporation takes place. Both plots for the droplet surface temperature and droplet radius are shown. The same values as shown in Table 4.2 for the initial droplet temperature, diameter, distance parameter and gas temperature are used, but in contrast to the case shown in Table 4.1, it is assumed that the droplet velocity remains constant and equal to 12.71 m/s. The cases of the stationary boundary during individual time steps, the cases when the effects of the moving boundary are taken into account for the heat transfer and species diffusion equations separately during individual time steps, and the case when these effects are taken into account simultaneously for heat transfer and species diffusion are shown.

As can be seen from this figure, the plots taking into account the effects of the moving boundary on the heat transfer equation only, and ignoring this effect altogether practically coincide. That means that this effect can be safely ignored for this case. Also, the plots taking into account the effects of the moving boundary on the solution to the species diffusion equation, and taking it into account for both solutions to the heat transfer and species diffusion equations practically coincide, but the difference between both these curves and the ones ignoring this effect altogether can be clearly seen after about 0.1 s. The effect of the moving boundary is a reduction of the predicted droplet surface temperature between about 0.1 to 0.6 s. During this period the droplet surface temperature is below the ambient gas temperature. Hence the reduction of the droplet surface temperature is expected to increase the heat flux from the ambient gas to the droplets, leading to the acceleration of droplet evaporation. This agrees with the predicted time evolution of the droplet radius, taking and not taking into account the effect of the moving boundary, shown in Fig. 4.6.

In Fig. 4.7 the case similar to the one shown in Fig. 4.6, but for gas temperature equal to 1000 K, is shown. In this case, droplet surface temperature increases during the whole period of droplet heating and evaporation, in contrast to the case shown in Fig. 4.6. As one can see from Fig. 4.7, the plots taking into account the effects of the moving boundary on the solution to the heat transfer equation, and ignoring this effect altogether practically coincide, as in the case shown in Fig. 4.7. Also, similarly to the case shown in Fig. 4.6, the plots taking into account the effects of the moving boundary on the solution to the species diffusion equations, and taking it into account for both heat transfer and species diffusion equations practically coincide, but the difference between both these curves and the ones ignoring this effect altogether can be clearly seen after about 5 ms. This difference between the plots is much more visible than in the case shown in Fig. 4.6. As in the case shown in Fig. 4.6, the effect of the moving boundary is to reduce the predicted droplet surface temperature leading to the increase of the heat flux from the ambient gas to the droplets and acceleration of droplet evaporation. This agrees with the predicted time evolution of droplet radius, taking and not taking into account the effect of the moving boundary, shown in Fig. 4.7.

The plots of time evolution of the surface mass fraction of ethanol $Y_{l;s;eth}$ for the

Figure 4.7: The same as Fig. 4.6 but for the gas temperature equal to 1000 K.

same case as shown in Fig. 4.7, are shown in Fig. 4.8. Similarly to the case shown in Fig. 4.7, the main e ect of the moving boundary on the solution to the species di usion equation is its in uence on the values of $Y_{l;s;eth}$. This e ect leads to visible reductions of the values of $Y_{l;s;eth}$ until the complete evaporation of the droplet takes place.

4.5 Conclusions of Chapter 4

Two new solutions to the equation, describing the di usion of species during multi-component droplet evaporation, are suggested. The rst solution is the explicit analytical solution to this equation, while the second one reduces the solution of the di erential transient species di usion equation to the solution of the Volterra integral equation of the second kind. Both solutions take into account the e ect of the reduction of the droplet radius due to tion. dropletspecies

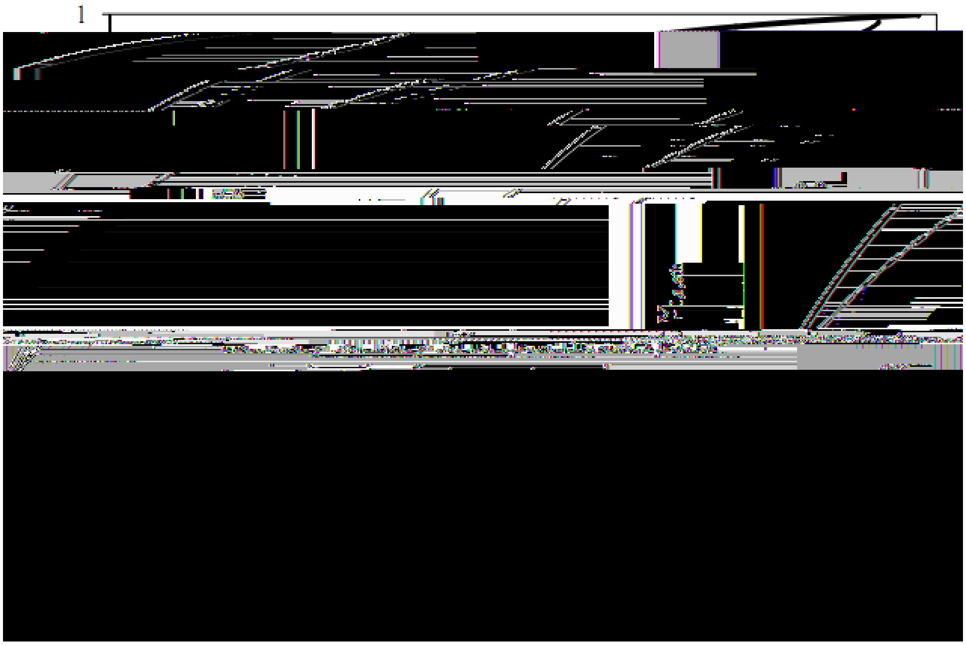

Figure 4.8: The same as Fig. 4.7 but for the mass fraction of ethanol at the surface of the droplet.

Chapter 2, which took into account the effect of the moving boundary due to droplet evaporation on the distribution of temperature inside the droplet.

The analytical solution has been incorporated into a zero dimensional CFD code and applied to the analysis of bi-component droplet heating and evaporation. The case of initial 50% ethanol – 50% acetone mixture and droplets with initial diameter equal to 142.7 μm, as in our earlier paper [38], has been considered. Effects of droplets on gas have been ignored at this stage and droplet velocity has been assumed to be constant and equal to 12.71 m/s. To separate the effect of the moving boundary on the species diffusion equation from similar effects on the heat conduction equation inside droplets, described in previous two Chapters, a rather artificial assumption that the droplet temperature is homogeneous and fixed has been made.

It has been pointed out that the moving boundary slows down the increase in the mass fraction of ethanol (the less volatile substance in the mixture) during the evaporation process and leads to the acceleration of droplet evaporation.

It is pointed out that for the conditions of the experiment described briefly earlier, species diffusion equations, are very close. The deviation between the predictions of these models can be ignored in this case. At the same time, the difference in the predictions of these models needs to be taken into account when the whole period of droplet evaporation up to the complete evaporation of droplets is considered. The effect of the moving boundary is shown to be much stronger for the solution to the species diffusion equation than for the solution to the heat conduction equation inside droplets.

Chapter 5

Transient heating of a semitransparent spherical body immersed into a gas with inhomogeneous temperature distribution

5.1 Introduction of Chapter 5

The main objective of this Chapter is to generalise the model described in [52] to the case when the initial gas temperature is not homogeneous in the vicinity of droplets.

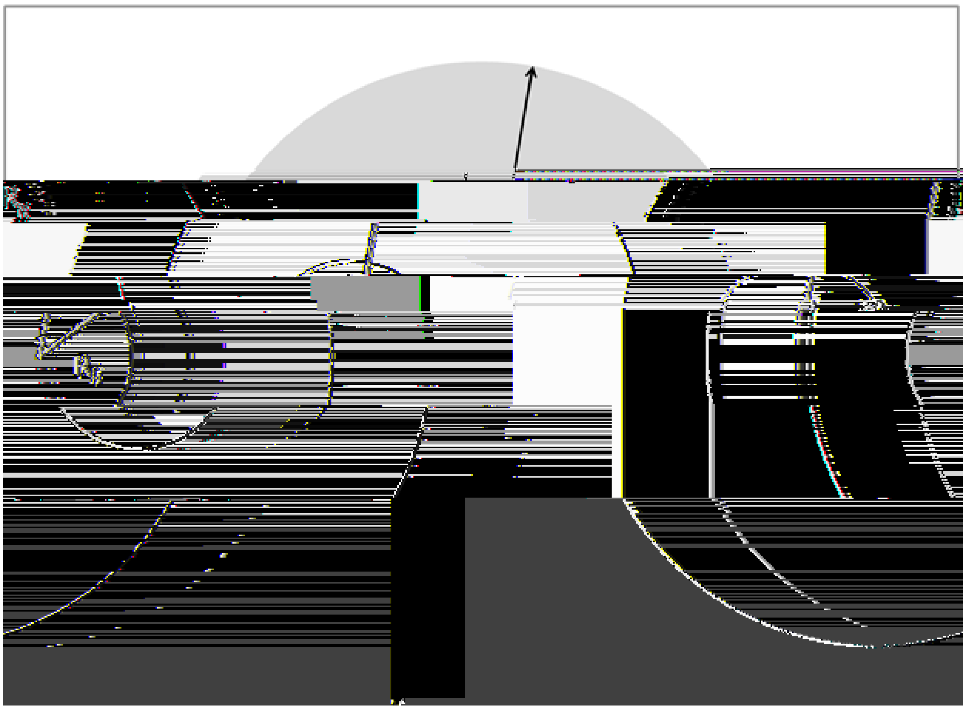

Figure 5.1: A schematic presentation of a spherical body of radius R_b immersed in the center of a gaseous sphere of radius R_g.

5.2 Basic equations and assumptions

As in [52], let us assume that a spherical body of radius R_b and initial temperature $T_{b0}(R)$ is immersed in the center of a gaseous sphere of radius R_g at temperature $T_{g0}(R)$, as schematically shown in Fig. 5.1. The outer surface temperature of the gaseous sphere remains constant and equal to $T_{g0}(R_g)$. R_g is greater than R_b but finite.

The variation of the temperatures in the gas-body domain is described by the heat conduction equation in the form [105, 106]:

$$\frac{\partial T}{\partial t} = \kappa \left(\frac{\partial^2 T}{\partial R^2} + \frac{2}{R}\frac{\partial T}{\partial R} \right) + P(t;R), \tag{5.1}$$

where

$$\kappa = \begin{cases} \kappa_b = k_b/(c_b \rho_b) & \text{when } R \le R_b \\ \kappa_g = k_g/(c_{pg} \rho_g) & \text{when } R_b < R \le R_g, \end{cases} \tag{5.2}$$

$T(R_g) = T_{g0}(R_g) = \text{const}$.

Equation (5.1) is identical to Equation (2.1). In contrast to Equation (2.1), however, κ in Equation (5.1) is not constant and the latter Equation refers to both liquid and gas. Equation (5.1) is the same as used in [52] except that T_{g0} is not constant but depends on R in the range $R_b < R \quad R_g$. The model for the radiation term $P(t; R)$ is the same as used in [52].

As in [52], Equation (5.1) needs to be solved subject to initial and boundary conditions:

$$T|_{t=0} = \begin{cases} T_{b0}(R) & \text{when} \quad R \quad R_b \\ T_{g0}(R) & \text{when} \quad R_b < R \quad R_g; \end{cases} \tag{5.3}$$

$$T|_{R=R_b} = T|_{R=R_b^+}; \quad k_b \left.\frac{\partial T}{\partial R}\right|_{R=R_b} = k_g \left.\frac{\partial T}{\partial R}\right|_{R=R_b^+}; \quad T|_{R=R_g} = T_{g0}(R_g). \tag{5.4}$$

The physical meaning of the value of $R_g \quad R_b$ can be interpreted in terms of the so called ` lm' theory [44]. The key concept of this theory is thermal lm thickness $_T$, the expression for which is derived from the requirement that the rate of a purely molecular transport by thermal conduction through the lm must be equal to the actual intensity of the convective heat transfer between the body surface and the external ow. For the case of heat conduction at the surface of a sphere this requirement can be written as [131]:

$$q_s'' = \frac{k_g \quad T}{R_b \quad \frac{R_b^2}{R_b + \ _{T0}}} = h \quad T; \tag{5.5}$$

where $q_s'' = |q_s|/(4 \ R_b^2)$ is the value of the heat ux at the surface of the droplet, $T = T_g \quad T_s$, index $_0$ here indicates that the e ects of the Stefan Tf 259.764.72gf 5.8533ects 92 (R_g) $_g$ T $_{g0}$

The introduction of non-zero Re affects our earlier assumption about the spherical symmetry of the problem and $h = k_g/R_b$. This can be overcome if we replace k_g by

$$k_{g,\mathrm{eff}} = k_g \mathrm{Nu}_0/2$$

to satisfy Equation (5.5). If the body is liquid then k_b would need to be replaced by the effective liquid thermal conductivity, following the effective thermal conductivity model [44]. These effects are not considered in this Chapter.

Note that the 'film theory' based on Equations (5.5)-(5.8) was developed under

$$||v_n||^2 = \frac{c_b\rho_b R_b}{2\sin^2(\lambda_n a_b R_b)} + \frac{c_{pg}\rho_g(R_g-R_b)}{2\sin^2(\lambda_n a_g(R_b-R_g))} - \frac{k_b-k_g}{2R_b\lambda_n^2};$$

$$p_n(t) = \frac{c_b\rho_b}{||v_n||^2}\int_0^{R_b} RP(t;R)v_n(R)\mathrm{d}R.$$

A countable set of positive eigenvalues λ_n is found from the solution to the equation:

$$\sqrt{k_b c_b\rho_b}\cot(\lambda a_b R_b) - \sqrt{k_g c_{pg}\rho_g}\cot(\lambda a_g(R_b-R_g)) = \frac{k_b-k_g}{R_b\lambda}. \tag{5.11}$$

These are arranged in ascending order $0<\lambda_1<\lambda_2<\ldots$. $a_b=\sqrt{\frac{c_b\rho_b}{k_b}}$, $a_g=\sqrt{\frac{c_{pg}\rho_g}{k_g}}$.

Having introduced new dimensionless variables:

$$\bar{T} = \frac{T(R;t)}{T_{g0}(R_g)};\quad \bar{T}_b = \frac{T_{b0}(R)}{T_{g0}(R_g)};\quad \bar{T}_g = \frac{T_{g0}(R)}{T_{g0}(R_g)};\quad r=\frac{R}{R_b};\quad r_g=\frac{R_g}{R_b};$$

and ignoring the contribution of thermal radiation, Equation (5.9) can be simplified to

$$\bar{T} = 1+\frac{R_b}{r}\sum_{n=1}^{\infty}\left[\exp\left(-\lambda_n^2 t\right)\frac{1}{||v_n||^2}\left(\int_0^1(-(1-\bar{T}_b)rv_n(R_b r)c_b\rho_b\mathrm{d}r\right.\right.$$

$$\left.\left.+\int_1^{r_g}(-(1-\bar{T}_g)rv_n(R_b r)c_{pg}\rho_g\mathrm{d}r\right)\right]v_n(R_b r); \tag{5.12}$$

If $T_{g0}(R)=T_{g0}(R_g)=$const and T_{b0} does not depend on R then Equation (5.9) can be simplified to

$$T(R;t) = T_{g0}+\frac{1}{R}\sum_{n=1}^{\infty}\left[\exp\left(-\lambda_n^2 t\right)\frac{(T_{g0}-T_{b0})\sqrt{k_b c_b\rho_b}}{\lambda_n||v_n||^2}\left(R_b\cot(\lambda_n a_b R_b)-\frac{1}{\lambda_n a_b}\right)\right.$$

$$\left.+\int_0^t\exp\left(-\lambda_n^2(t-\tau)\right)p_n(\tau)\mathrm{d}\tau\right]v_n(R). \tag{5.13}$$

This solution was studied in detail in the previous paper [52].

5.4 Analysis

Let us consider typical values of parameters for the case when Diesel fuel droplets with an initial temperature of 300 K are injected into a gas at temperature 900 K and pressure 30 atm (situation typical for Diesel engines [42]):

$$\rho_b = 600\ \ \mathrm{kg/m^3}\quad k_b = 0.145\ \ \mathrm{W/(mK)}\quad c_b = 2830\ \ \mathrm{J/(kgK)}$$

$$\rho_g = 23.8\ \ \mathrm{kg/m^3}\quad k_g = 0.061\ \ \mathrm{W/(mK)}\quad c_{pg} = 1120\ \ \mathrm{J/(kgK)}.$$

This leads us to the following estimates of thermal diffusivities of the body and gas as defined by Equation (5.2):

$$\kappa_b = 8.54 \times 10^{-8}\ \mathrm{m^2/s}; \qquad \kappa_g = 2.29 \times 10^{-6}\ \mathrm{m^2/s}.$$

Note that we took gas temperature slightly higher than the one used in [52], where it was assumed that $T_{g0}(R_g) = 800$ K. The values of transport coefficients for gas were taken to be the same as in [42, 52]. The difference of the values of these coefficients for these two temperatures were ignored as in [52].

We assume that the droplets can be treated as a body the temperature of which is initially homogeneous, while $T_{g0}(R_g) = 900$ K and $R_b = 10\ \mu$m. Pr is assumed to be equal to 0.7 and two values of Re are considered: 1 and 5. Remembering (5.6), this leads to the following values of R_g:

$$R_{g1} = 3.301\, R_b \quad \text{and} \quad R_{g2} = 11.337\, R_b.$$

Two cases of the initial distribution of gas temperature in the range $R_b < R \leq R_g$ are considered. Firstly, we assume that $T_{g0}(R)$ satisfies Equation (5.8), which leads to the following expression:

$$T_{g0}(R) = T_{b0} + [T_{g0}(R_g) - T_{b0}]\, \frac{\frac{1}{R_b} - \frac{1}{R}}{\frac{1}{R_b} - \frac{1}{R_g}}. \tag{5.14}$$

Secondly we assume that

$$T_{g0}(R) = T_{g0}(R_g). \tag{5.15}$$

The latter case is identical to the one considered in [52].

The analysis of the effects of thermal radiation would lead to the results identical to the ones reported in [52]. This will not be considered in this work.

The analysis will be focused on the dimensionless time (Fourier number), distance and temperature defined as:

$$\mathrm{Fo} = t\,\kappa_g/R_b^2; \quad r = R/R_b; \quad \hat{T}_{(s)} = (T_{g0}(R_g) - T_{(s)}(R;t))/(T_{g0}(R_g) - T_{b0}).$$

The calculations were performed using the package Wolfram Mathematica v 6.0 on a one 3.0 GHz Kernel. 100 terms of the series were taken.

Plots of $\hat{T}$

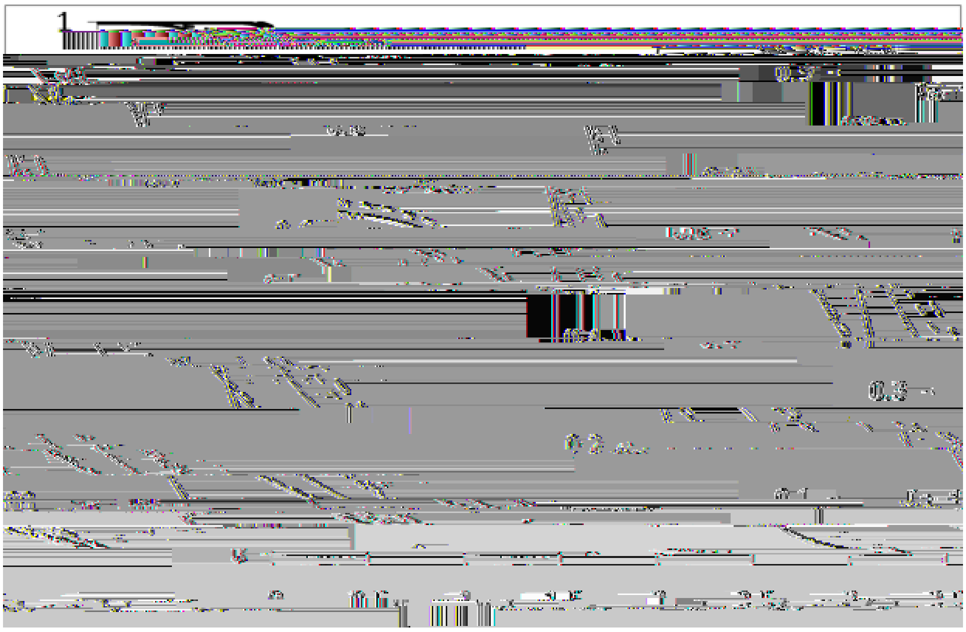

Figure 5.2: The plots of $\hat{T}$ $(T_{g0}(R_g)$ $T(R;t))=(T_{g0}(R_g)$ $T_{b0})$ versus $r = R=R_b$ for r_g $R_g=R_b = 3{:}301$ and four Fo (indicated near the curves). Solid curves refer to the initial distribution (5.15), while dashed curves refer to the initial distribution (5.14). The thickness of the curves is inversely proportionate to Fo.

by Expressions (5.14) and (5.15). As follows from this gure, for Fo $= 0{:}1$ most of the interior of the body is not a ected by high gas temperature for both initial distributions of $T_{g0}(R)$, but the body temperatures near the surface are a ected stronger by gas for distribution (5.15), compared with distribution (5.14). The di erence in gas temperatures (f 3.251 0 Td [(1) -414/F23 7.9701 Tr Fo (indicatedg

1

Figure 5.3: The same as Fig. 5.2 but for $r_g = 11{:}337$.

The plots of $\hat{T}_s$ versus Fo for $R_g = 3{:}301\,R_b$, $R_g = 11{:}337\,R_b$ and both initial distributions of $T_{g0}(R)$ are shown in Fig. 5.4. As follows from this gure, the body surface is always heated quicker for distribution (5.15) compared with distribution (5.14) as expected. Also, the body is heated quicker for $R_g = 3{:}301\,R_b$ than for $R_g = 11{:}337\,R_b$. All these results are consistent with those shown in Figs. 5.2 and

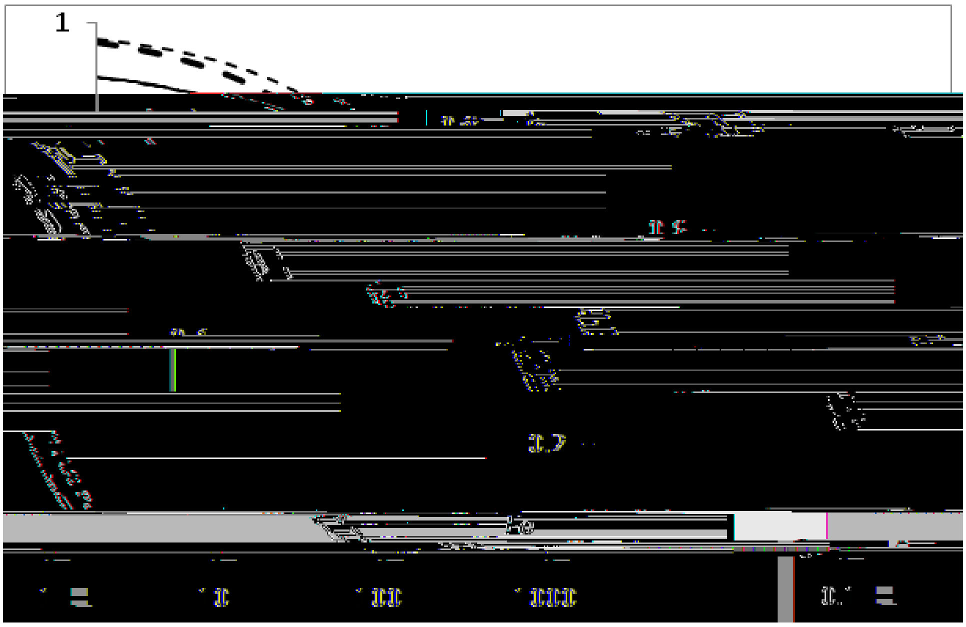

Figure 5.4: The plots of $\hat{T}_s$ $(T_{g0}(R_g)$ $T_s(R;t))=(T_{g0}(R_g)$ $T_{b0})$ versus Fo for r_g = 3:301 and distribution (5.15) (solid), r_g = 11:337 and distribution (5.15) (dashed-dotted), r_g = 3:301 and distribution (5.14) (thick dashed), r_g = 11:337 and distribution (5.14) (thin dashed).

If the Newton's law is valid then = 1. As shown in [52] for the special case of a body immersed into a homogeneous gas, this is not valid in the general transient case.

The plots of versus Fo for various r_g R_g=R_b, and both initial distributions of $T_{g0}(R$

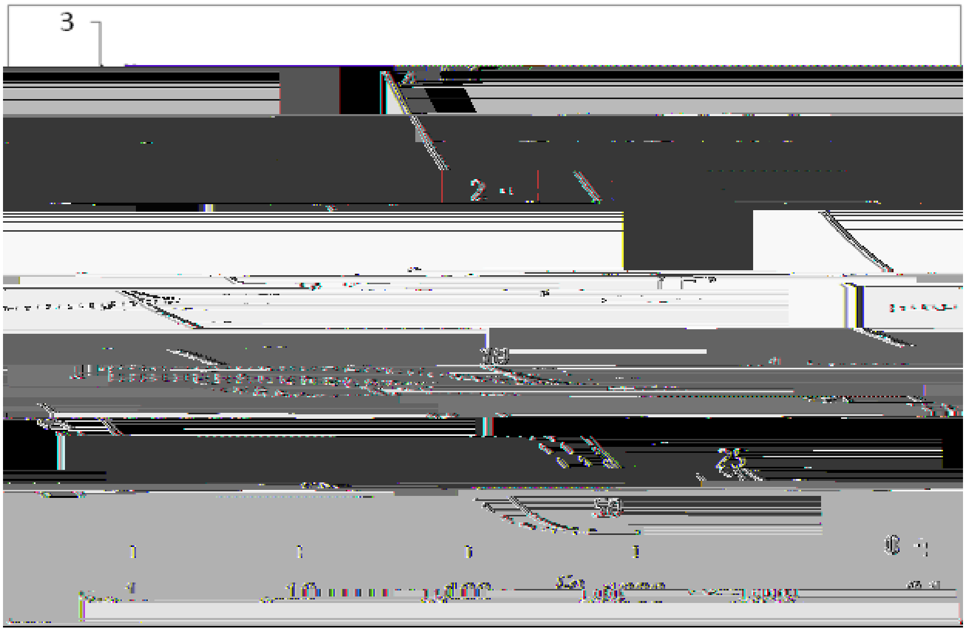

Figure 5.5: The plots of

on the distance from the body surface, if this distance is less than $R_g \quad R_b$. The solution is applied to modelling body heating in conditions close to those observed in Diesel engines.

It is pointed out that inhomogeneous gas temperature distribution leads to slowing down of body heating compared with the case when the body is immersed into a homogeneous gas. In the long time limit, the distribution of temperature in the body and gas practically does not depend on the initial distribution of gas temperature.

The study of the correction of the convective heat transfer coe cient for the case of body immersion in gas with homogeneous temperature distribution con rmed the results earlier reported in [52]. For small Fo, this correction does not depend on the size of the gas domain, and reaches about 2.8 at Fo $= 0{:}1$. For Fo > 1 this correction becomes sensitive to the size of the domain. For large domains it has e s o-288(it,o27aF-288e]T

Chapter 6

Conclusions

New solutions to the heat conduction equation, describing transient heating of an evaporating droplet, are suggested. These solutions take into account the e ect of the reduction of the droplet radius due to evaporation, assuming that this radius is a linear function of time. The latter assumption does not allow us to apply these solutions to describe the whole process, from the start of evaporation, until the moment in time when the droplet completely evaporates. However, these solutions are expected to be used to describe droplet heating and evaporation over a small time step when other parameters, except droplet radius and temperature, can be assumed constant. In this case they can be considered as generalisations of the approach

the distance from the droplet centre, predict the same results. This suggests that both models are likely to be correct. It is shown that the temperatures predicted by the models based on the assumption of constant initial droplet temperature, and the one taking into account the increase in this temperature with the distance from the droplet centre, tend to converge with time.

Two new solutions to the equation, describing the diffusion of species during multi-component droplet evaporation, are suggested. Both solutions take into account the effect of the reduction of the droplet radius due to evaporation, assuming that this radius is a linear function of time. The first solution is the explicit analytical solution to this equation, while the second one reduces the solution of the differential the species di usion equation than for the solution to the heat conduction equation inside droplets.

The problem of heating of a body immersed into gas with inhomogeneous temperature distribution is solved analytically assuming that at a certain distance R_g R_b from the body gas temperature remains constant. This problem is the generalisation of the problem solved earlier when gas, into which the body is immersed, is assumed to be initially homogeneous. This solution is applied to the case when the distribution of gas temperature is chosen such that heat ux in gas initially does not depend on the distance from the body surface, if this distance is less than R_g R_b. The solution is applied to modelling body heating in conditions close to those observed in Diesel engines.

It is pointed out that inhomogeneous gas temperature distribution leads to slowing down of body heating compared with the case when the body is immersed into a homogeneous gas. In the long time limit, the distribution of temperature in the body and gas practically does not depend on the initial distribution of gas temperature. The study of the correction of the convective heat transfer coe cient for the case of body immersion in gas with homogeneous temperature distribution con rmed the results earlier reported in [52]. For small Fo, this correction does not depend on the size of the gas domain, and reaches about 2.8 at Fo $= 0.1$. For Fo > 1 this correction becomes sensitive to the size of the domain. For large domains it has been shown to be the same as follows from the earlier model suggested in [67] for an in nitely large domain occupied by the gas. The values of this correction to Newton's law vary from about 0.1 8(hes)-s27(t8(o)1(ut)-284g)-28dyb th2 pr2 ga

References

[1] S.S. Sazhin. Advanced models of fuel droplet heating and evaporation. *Progress in Energy and Combustion Science*, 32(2):162–214, 2006.

[2] S.S. Sazhin, I.N. Shishkova, and M.R. Heikal. Kinetic modelling of fuel droplet heating and evaporation: calculations and approximations. *International Journal of Engineering Systems Modelling and Simulation*, 2(3):169–176, 2010.

[3] B.Y. Cao, J.F. Xie, and S.S. Sazhin. Molecular dynamics study on evaporation and condensation of n-dodecane at liquid–vapor phase equilibria. *The Journal of Chemical Physics*, 134:164309, 2011.

[4] J.F. Xie, S.S. Sazhin, and B.Y. Cao. Molecular dynamics study of the processes in the vicinity of the n-dodecane vapour/liquid interface. *Physics of Fluids*, 23:112104, 2011.

[5] I.N. Shishkova and S.S. Sazhin. A numerical algorithm for kinetic modelling of evaporation processes. *Journal of Computational Physics*, 218(2):635–653, 2006.

[6] S.S. Sazhin, I.N. Shishkova, A.P. Kryukov, V.Y. Levashov, and M.R. Heikal. Evaporation of droplets into a background gas: Kinetic modelling. *International Journal of Heat and Mass Transfer*, 50:2675–2691, 2007.

[7] S.S. Sazhin, I.N. Shishkova, T. Kristyadi, S.P. Martynov, and M.R. Heikal. Droplet heating and evaporation: hydrodynamic and kinetic models. *Heat Transfer Research*, 39(4):293–303, 2008.

[8] S.S. Sazhin and I.N. Shishkova. A kinetic algorithm for modelling the droplet

evaporation process in the presence of heat ux and background gas. *Atomi-zation and Sprays*, 19:473{489, 2009.

[9]

[19] S.S. Sazhin, P.A. Krutitskii, I.G. Gusev, and M.R. Heikal. Transient heating of an evaporating droplet. *International Journal of Heat and Mass Transfer*, 53:2826–2836, 2010.

[20] S.S. Sazhin, P.A. Krutitskii, I.G. Gusev, and M.R. Heikal. Transient heating of an evaporating droplet with presumed time evolution of its radius. *International Journal of Heat and Mass Transfer*, 54(5-6):1278–1288, 2011.

[21] I.G. Gusev, P.A. Krutitskii, S.S. Sazhin, and A.E. Elwardany. New solutions

[27] S.S. Sazhin, A. Elwardany, I.G. Gusev, I.N. Shishkova, and M. Heikal. Modelling of fuel droplet heating and evaporation: recent results and unsolved problems. In *Engineering Research Anniversary meeting Amalia and Miklos Lajin*, pages pp. B:197{B:209, University of Pecs, Hungary, October 25-26 2010. Pollack Mihaly Faculty of Engineering, University of Pecs.

[28] I.G. Gusev, P.A. Krutitskii, and S.S. Sazhin. Droplet heating and evaporation in the presence of a moving boundary: numerical analysis based on analytical solutions. In *Book of Abstracts*, page 42, University of Brighton (UK), 12-14th July 2010. 11th International Conference on Integral Methods in Science and Engineering.

[29] S.S. Sazhin, I.N. Shishkova, I.G. Gusev, A. Elwardany, P.A. Krutitskii, and M. Heikal. Fuel droplet heating and evaporation: new hydrodynamic and kinetic models. In *Book of Abstracts*, page 26, Washington, 8-13 August 2010. 11th International Conference on Integral Methods in Science and Engineering.

[30] S.S. Sazhin, I.N. Shishkova, I.G. Gusev, and M. Heikal. Hydrodynamic and kinetic models for monocomponent droplet heating and evaporation: recent developments. In *Book of Abstracts*, page 183, Kaohsiung City, Taiwan, 2-5 November 2010. 21st International Symposium on Transport Phenomena.

[31] S.S. Sazhin, A. Elwardany, I.G. Gusev, J.-F. Xie., B.-Y Cao, I.N. Shishkova, A.Yu. Snegirev, and M. Heikal. Modelling of complex hydrocarbon droplet heating and evaporation: hydrodynamic, kinetic and molecular dynamics approaches. In *Book of Abstracts*, Saint Petersburg, Russia, June 24-27 2011. 25th European Symposium on Applied Thermodynamics.

[32] I.G. Gusev, S.S. Sazhin, and M. Heikal. The effects of the moving boundary on the heating of evaporating droplets. In *Proceedings of ILASS Europe 2011*, page 119, Estoril, Portugal, 5-7 September 2011. 24th European Conference on Liquid Atomization and Spray Systems.

[33] S.S. Sazhin, I.G. Gusev, M. Heikal, and P.A. Krutitskii. Modelling of liquid droplet heating and evaporation taking into account the effects of the moving boundary. In *Program and Book of Abstracts*, page 75, Kyoto, 22{26 September

2011. The Asian Symposium on Computational Heat Transfer and Fluid Flow - 2011 (ASCH2011).

[34] G. Miliauskas. Regularities of unsteady radiative?onductive heat transfer in evaporating semitransparent liquid droplets. *International Journal of Heat and Mass Transfer*, 44:785{798, 2001.

[35] A.D. Polyanin, A.M. Kutepov, A.V. Vyazmin, and D.A. Kazenin. *Hydrodynamics, Mass and Heat Transfer in Chemical Engineering*. Taylor & Francis, 2002.

[36] A. Faghri and Y. Zhang. *Transport Phenomena in Multiphase Systems*. Academic Press, 2006.

[37] S. Sazhin. Modelling of sprays using computational uid dynamics codes. *Polytechnica Periodica*, 4(1):5{16, 2009.

[38] S.S. Sazhin, A. Elwardany, P.A. Krutitskii, G. Castanet, F. Lemoine, E.M. Sazhina, and M.R. Heikal. A simpli ed model for bi-component droplet heating and evaporation. *International Journal of Heat and Mass Transfer*, 53(21-22):4495{4505, 2010.

[39]

[43] V. Bykov, I. Goldfarb, V. Goldshtein, and J.B. Greenberg. Thermal explosion in a hot gas mixture with fuel droplets: a two reactant model. *Combustion Theory and Modelling*, 6(2):339{359, 2002.

[44] B. Abramzon and W.A. Sirignano. Droplet vaporization model for spray combustion calculations. *International Journal of Heat and Mass Transfer*, 32(9):1605{1618, 1989.

[45] R.J. Haywood, R. Nafziger, and M. Renksizbulut. A detailed examination of gas and liquid transient processes in convection and evaporation. *ASME Journal Heat Transfer*, 111:495{502, 1989.

[46] C.H. Chiang, M.S. Raju, and W.A. Sirignano. Numerical analysis of convecting, vaporizing fuel droplet with variable properties. *International Journal of Heat and Mass Transfer*, 35(5):1307{1324, 1992.

[47] E.M. Sazhina, S.S. Sazhin, M.R. Heikal, V.I. Babushok, and R.J.R. Johns. A detailed modelling of the spray ignition process in diesel engines. *Combustion Science and Technology*, 160(1):317{344, 2000.

[48] G. Castanet, M. Lebouche, and F. Lemoine. Heat and mass transfer of combusting monodisperse droplets in a linear stream. *International Journal of Heat and Mass Transfer*, 48:3261{3275, 2005.

[49] C. Maqua, G. Castanet, F. Grisch, F. Lemoine, T. Kristyadi, and S.S. Sazhin. Monodisperse droplet heating and evaporation: experimental study and modelling. *International Journal of Heat and Mass Transfer*, 51(15-16):3932{3945, 2008.

[50] S.S. Sazhin, A.E. Elwardany, P.A. Krutitskii, V. Depredurand, G. Castanet, F. Lemoine, E.M. Sazhina, and M.R. Heikal. Multi-component droplet heating and evaporation: Numerical simulation versus experimental data. *International Journal of Thermal Sciences*, 50(7):1164{1180, 2011.

[51] C. Bertoli and M. Migliaccio. Finite conductivity model for diesel spray evaporation computations. *International Journal of Heat and Fluid Flow*, 20(5):552{561, 1999.

[52] S.S. Sazhin, P.A. Krutitskii, S.B. Martynov, D. Mason, M.R. Heikal, and E.M. Sazhina. Transient heating of a semitransparent spherical body. *International Journal of Thermal Sciences*, 46(5):444–457, 2007.

[53] R.B. Bird, W.E. Stewart, and E.N. Lightfoot. *Transport Phenomena*. John Wiley & Sons, Chichester, 2002.

[54] G. Brenn. Concentration fields in evaporating droplets. *International Journal of Heat and Mass Transfer*, 48:395–402, 2005.

[55] C. Maqua, G. Castanet, and F. Lemoine. Bi-component droplets evaporation: temperature measurements and modelling. *Fuel*, 87:2932–2942, 2008.

[56] G.M. Faeth. Evaporation and combustion of sprays. *Progress in Energy and Combustion Science*, 9(1-2):1–76, 1983.

[57] A.Y. Tong and W.A. Sirignano. Multicomponent transient droplet vaporization with internal circulation: integral equation formulation and approximate solution. *Numerical Heat Transfer*, 10(3):253–278, 1986.

[58] G. Continillo and W.A. Sirignano. Unsteady, spherically-symmetric flame propagation through multicomponent fuel spray clouds. In *Modern research topics in aerospace propulsion (In honor of Corrado Casci) (A 91-45656 19-31)*, volume 1, pages 173–198. New York, Springer-Verlag, 1991.

[59] M. Klingsporn and U. Renz. Vaporization of a binary unsteady spray at high temperature and high pressure. *International Journal of Heat and Mass Transfer*, 37:265–272, 1994.

[60] P.L.C. Lage, C.M. Hackenberg, and R.H. Rangel. Nonideal vaporization of dilating binary droplets with radiation absorption. *Combustion and Flame*, 101:36–44, 1995.

[61] D.J. Torres, P.J. O'Rourke, and A.A. Amsden. Efficient multicomponent fuel algorithm. *Combustion Theory and Modelling*, 7(1):67–86, 2003.

[62] J. Tamim and W.L.H. Hallett. A continuous thermodynamics model for multi-component droplet vaporization. *Chemical Engineering Science*, 50(18):2933–2942, 1995.

[63] A.M. Lippert and R.D. Reitz. Modeling of Multicomponent Fuels Using Continuous Distributions With Application to Droplet Evaporation and Sprays. *SAE Technical Paper*, SP-1306:No. 972882, 1997.

[64] G-S. Zhu, R.D. Reitz, and Aggarwal S.K. Gas-phase unsteadiness and its in uence on droplet vaporization in sub- and super-critical environments. *International Journal of Heat and Mass Transfer*, 44:3081{93, 2001.

[65] M. Burger, R. Schmehl, K. Prommersberger, O. Schfer, R. Koch, and S. Wittig. Droplet evaporation modelling by the distillation curve model: accounting for kerosene fuel and elevated pressures. *International Journal of Heat and Mass Transfer*, 46:4403{4411

[73] E. Loth. Numerical approaches for motion of dispersed particles, droplets and bubbles. *Progress in Energy and Combustion Science*, 26(3):161{223, 2000.

[74] M. Orme. Experiments on droplet collisions, bounce, coalescence and disruption. *Progress in Energy and Combustion Science*, 23(1):65{79, 1997.

[75] H.A. Dwyer, P. Stapf, and R. Maly. Unsteady vaporization and ignition of a three-dimensional droplet array. *Combustion and Flame*, 121(1-2):181{194, 2000.

[76] K. Harstad and J. Bellan. Evaluation of commonly used assumptions for

[84] R.T. Imaoka and W.A. Sirignano. A generalized analysis for liquid-fuel vaporization and burning. *International Journal of Heat and Mass Transfer*, 48(21):4342{4353, 2005.

[85] R.T. Imaoka and W.A. Sirignano. Transient vaporization and burning in dense droplet arrays. *International Journal of Heat and Mass Transfer*, 48(21):4354{4366, 2005.

[86] S.G. Kandlikar and M.E. Steinke. Contact angles and interface behavior during rapid evaporation of liquid on a heated surface. *International Journal of Heat and Mass Transfer*, 45:3771{80, 2002.

[87] S.C. Li. Spray stagnation ames. *Progress in Energy and Combustion Science*, 23(4):303{347, 1997.

[88] C.H. Tsai, S.S. Hou, and T.H. Lin. Spray ames in a one-dimensional duct of varying cross-sectional area. *International Journal of Heat and Mass Transfer*, 48(11):2250{2259, 2005.

[89] C. Crua, D.A. Kennaird, S.S. Sazhin, M.R. Heikal, and M.R. Gold. Diesel autogignition at elevated in-cylinder pressueres. *International Journal of Engine Research*, 5(4):365{374, 2004.

[90] S.S. Sazhin, E.M. Sazhina, and M.R. Heikal. Modelling of the gas to fuel droplets radiative exchange. *Fuel*, 79(14):1843{1852, 2000.

[91] L.A. Dombrovsky, S.S. Sazhin, E.M. Sazhina, G. Feng, M.R. Heikal, M.E.A. Bardsley, and S.V. Mikhalovsky. Heating and evaporation of semi-transparent diesel fuel droplets in the presence of thermal radiation. *Fuel*, 80(11):1535{1544, 2001.

[92] L.A. Dombrovsky, S.S. Sazhin, S.V. Mikhalovsky, R. Wood, and M.R. Heikal. Spectral properties of diesel fuel droplets. *Fuel*, 82(1):15{22, 2003.

[93] L. Dombrovsky and S. Sazhin. Absorption of thermal radiation in a [(I0 g 0 G [-489

[94] S.S. Sazhin, W.A. Abdelghaffar, E.M. Sazhina, SV Mikhalovsky, S.T. Meikle, and C. Bai. Radiative heating of semi-transparent diesel fuel droplets. *Journal of Heat Transfer*, 126:105, 2004.

[95] L. Dombrovsky and S. Sazhin. Absorption of external thermal radiation in asymmetrically illuminated droplets. *Journal of Quantitative Spectroscopy and Radiative Transfer*, 87(2):119–135, 2004.

[96] B. Abramzon and S. Sazhin. Convective vaporization of a fuel droplet with thermal radiation absorption. *Fuel*, 85(1):32–46, 2006.

[97] S.S. Sazhin, T. Kristyadi, W.A. Abdelghaffar, S. Begg, M.R. Heikal, S.V. Mikhalovsky, S.T. Meikle, and O. Al-Hanbali. Approximate analysis of thermal radiation absorption in fuel droplets. *Journal of Heat Transfer*, 129:1246, 2007.

[98] Ch Soret. Sur l'etat d'equilibre que prend au poin de vue de sa concentration une dissolution saline primitivement homogene dont deux parties sont portees a des temperatures differentes. *Archives des Sciences Physiques et Naturelles*, 2:48–61, 1879.

[99] S.R. de Groot and P. Mazur. *Non-equilibrium Thermodynamics*. Amsterdam: North-Holland Publishing Company, 1962.

[100] R.M.L. Coelho and A. Silva Telles. Extended graetz problem accompanied by dufour and soret effects. *International Journal of Heat and Mass Transfer*, 45(15):3101–3110, 2002.

[101] A. Postelnicu. Influence of a magnetic field on heat and mass transfer by natural convection from vertical surfaces in porous meadia considering Soret and Dufour effects. *International Journal of Heat and Mass Transfer*, 47:1467–72, 2004.

[102] V. Gopalakrishnan and J. Abraham. Effects of multicomponent diffusion on predicted ignition characteristics of an n-heptane diffusion flame. *Combustion and Flame*, 136:557–566, 2004.

[113] S. Savovic and J. Caldwell. Finite-difference solution of one-dimensional Stefan problem with periodic boundary conditions. *International Journal of Heat and Mass Transfer*, 46:2911–2916, 2003.

[114] S. Kutluay, A.R. Bahadir, A. Ozdes, S. Kutluay, AR Bahadir, and A. Özdes. The numerical solution of one-phase classical stefan problem. *Journal of Computational and Applied Mathematics*, 81(1):135–144, 1997.

[115] P.C. Meek and J. Norbury. Nonlinear moving boundary problems and a Keller box scheme. *SIAM Journal on Numerical Analysis*, 21:883–893, 1984.

[116] S.L. Mitchell and M. Vynnycky. Finite-difference methods with increased accuracy and correct initialization for one-dimensional Stefan problems. *Applied*

metries. *Communications in Numerical Methods in Engineering*, 16:569{583, 2000.

[123] J. Caldwell and C.K. Chiu. Numerical solution of one-phase Stefan problems by the heat balance integral method, Part II - special small time starting procedure. *Communications in Numerical Methods in Engineering*, 16:585{593, 2000.

[124] T.R. Goodman. The heat-balance integral and its application to problems involving a change of phase. *Transactions of the ASME Journal*, 80(2):335{342, 1958.

[125] S.L. Mitchell and T.G. Myers. A heat balance integral method for one-dimensional nite ablation. *AIAA Journal Thermophysics and Heat Transfer*, 22(2): 508{514, 2008.

[126] S.L. Mitchell and T.G. Myers. Approximate solution methods for one-dimensional solidi cation from an incoming uid. *Applied Mathematics and Computation*, 202(1):311{326, 2008.

[127] T.G. Myers, S.L. Mitchell, G. Muchatibaya, and M.Y. Myers. A cubic heat balance integral method for one-dimensional melting of a nite thickness layer. *International Journal of Heat and Mass Transfer*, 50: 5305{5317, 2007.

[128] T.G. Myers. Optimizing the exponent in the heat balance and re ned integral methods. Submitted to Int. Comm. Heat & Mass Trans., 2008.

[129] S.L. Mitchell and T.G. Myers. Application of standard and re ned heat balance integral methods to one-dimensional Stefan problems. *SIAM Review*, 52(1): 57{86, 2010.

[130] A.N. Tikhonov and A.A. Samarsky. *Equations of Mathematical Physics*. Nauka Publishing House, 1972 (in Russian).

[131] F.P. Incropera and D.P. DeWitt. *Fundamentals of Heat and Mass Transfer*. John Wiley & Sons;, New York, 1996.

[132] V. S. Vladimirov. *Equations of Mathematical Physics*. Marcel Dekker, N, 1971.

Appendices

Appendix 1

Convergence of the Series in $G_1(t;\tau;\lambda)$ and Estimate of $G_1(t;\tau;\lambda)$ at $t-\tau\to 0$

Let us assume that

$$0 \le \tau \le t < t_e = -1/\lambda$$

and introduce the new function:

$$f(t;\tau) \equiv \frac{1}{R_{d0}}\left(\frac{1}{R_d(t)} - \frac{1}{R_d(\tau)}\right) = \frac{t-\tau}{R_d(t)R_d(\tau)}. \qquad (A11)$$

In the case of a time step, t_e needs to be replaced by Δt. As it was done earlier, to simplify the notation it is assumed that t_0 (the start of the time step) is equal to zero. This comment and assumption apply to both Appendices 1 and 2. Note that

$$f(t;\tau) \ge \frac{t-\tau}{R_{d0}^2} \qquad (A12)$$

since $\lambda < 0$ and $R_d(t) \le R_{d0}$.

It follows from (2.31) and the estimate $\lambda_n > n\pi$ for $n > 1$ that $||v_n||^2 > 1/4$ for $n > 1$. Therefore:

$$||v_n||^2 \ge c_0; \quad n \ge 1; \qquad (A13)$$

where $c_0 = \min\{||v_1||^2; 1/4\}$ is a positive constant.

Condition (A12) allows us to make the following estimate:

$$\exp\left[-\lambda_n^2 f(t;\tau)\right] \le \exp\left[-n^2\pi^2\frac{t-\tau}{R_{d0}^2}\right]; \quad n > 1; \qquad (A14)$$

where we took into account that $\lambda_n > n\pi$ for $n > 1$ (see Equation (17) in [15]). Using (A14) one can conclude that the series in $G_1(t;\tau;\lambda)$ converges absolutely and uniformly to the continuous function for $(t-\tau;\xi) \in [\varepsilon; 1/\varepsilon) \times [0;1]$ for any small $\varepsilon > 0$ since:

$$\exp\left[-\lambda_n^2 \frac{t-\tau}{R_{d0}^2}\right] \le \exp\left[-\lambda_n^2 \frac{\varepsilon}{R_{d0}^2}\right]; \quad |\sin \lambda_n \xi| \le 1. \qquad (A15)$$

Indeed, each term with $n > 1$ in the series in $G_1(t;\tau;\xi)$ for $(t-\tau;\xi) \in [\varepsilon; 1/\varepsilon) \times [0;1]$ can be majorized by the corresponding term of the convergent number series

$$c_0^{-1} \exp\left(-\lambda_n^2 \frac{\varepsilon}{R_{d0}^2}\right).$$

Now we estimate $G_1(t;\tau;\xi)$ for small $t-\tau > 0$. Inequalities (A13) and (A14) allow us to write:

$$|G_1(t;\tau;\xi)| \le c_0^{-1}\left\{1 + \sum_{n=2}^{\infty} \exp\left[-\lambda_n^2 f(t;\tau)\right]\right\}$$

$$\le c_0^{-1}\left\{1 + \sum_{n=2}^{\infty} \exp\left[-\pi^2 n^2 (t-\tau)/R_{d0}^2\right]\right\} \equiv G(t-\tau). \qquad (A16)$$

The sum $\sum_{n=2}^{\infty} \exp[-\pi^2 n^2 (t-\tau)/R_{d0}^2]$ can be considered as a sum of areas of polygons of unit width placed under the curve $\exp[-\pi^2 y^2 (t-\tau)/R_{d0}^2]$. This sum is less than the area under this curve. Hence,

$$\sum_{n=2}^{\infty} \exp\left[-\pi^2 n^2 (t-\tau)/R_{d0}^2\right] < \int_1^{\infty} \exp\left[-\pi^2 y^2 (t-\tau)/R_{d0}^2\right] dy$$

$$< \int_0^{\infty} \exp\left[-\pi^2 y^2 (t-\tau)/R_{d0}^2\right] dy = \frac{R_{d0}}{\pi\sqrt{(t-\tau)}} \int_0^{\infty} \exp\left[-z^2\right] dz$$

$$= \frac{R_{d0}\sqrt{\pi}}{2\pi\sqrt{(t-\tau)}} \qquad (A17)$$

Having substituted (A17) into (A16) we obtain:

$$|G_1(t;\tau;\xi)| \le G(t-\tau) < c_0^{-1}\left[1 + \frac{R_{d0}\sqrt{\pi}}{2\pi\sqrt{(t-\tau)}}\right] < \tilde{c}/\sqrt{t-\tau}; \qquad (A18)$$

$$t-\tau \in (0; t_{00}];$$

for any small fixed $t_{00} \in (0; 1/\varepsilon)$. The new constant $\tilde{c}$ depends on t_{00}. Inequality (A18) holds uniformly for $\xi \in [0;1]$.

Appendix 2

Numerical solution of Equation (2.51)

Let $\varphi(t) \equiv W(t;1)$ and rewrite Equation (2.51) as:

$$\varphi(t) = V(t;1) - \int_0^t [\mu_0(\tau) - h_1(\tau)\varphi(\tau)]\, G(t;\tau;1)\,\mathrm{d}\tau \, . \qquad (A21)$$

We look for the solution of Equation (A21) for $t \in [0;\hat{t}]$, where $\hat{t}$ is a constant, $\hat{t} < t_e$. Let $\Delta t = \hat{t}/N$ and $t_n = n\Delta t$, where N is the total number of time steps, $n = 0;1;\ldots;N$ is the number of the current time step. Note that $t_0 = 0$ and $t_N = \hat{t}$. Discretisation of Equation (A21) gives:

$$\varphi(t_n) = V(t_n;1) - \sum_{j=1}^{n} \int_{t_{j-1}}^{t_j} [\mu_0(\tau) - h_1(\tau)\varphi(\tau)]\, G(t_n;\tau;1)\,\mathrm{d}\tau \, , \qquad (A22)$$

where $n = 1;\ldots;N$. Note that $\varphi(t_0) = \varphi(0) = V(0;1) = W_0(1)$ is a known constant.

The first $(n-1)$ integrals in this sum can be approximated as:

$$\int_{t_{j-1}}^{t_j} [\mu_0(\tau) - h_1(\tau)\varphi(\tau)]\, G(t_n;\tau;1)\,\mathrm{d}\tau$$

$$\approx \{\mu_0(\tau_j) - h_1(\tau_j)[\varphi(t_j) + \varphi(t_{j-1})]/2\}\, G(t_n;\tau_j;1)\,\Delta t, \qquad (A23)$$

where $j = 1;2;\ldots;n-1$, $\tau_j = t_j - \frac{1}{2}\Delta t$. Approximation (A23) is valid since all functions in the integrand are continuous and we look for the solution in the class of continuous functions.

In Approximation (A23) the known functions are taken at $\tau = \tau_j$ (middle of the range $[t_{j-1};t_j]$), while the unknown functions are taken as the average of the values at the end points t_{j-1} and t_j.

The last term in the sum in Equation (A22) requires special investigation since the kernel $G(t_n;\tau;1)$ in the integrand becomes singular when $\tau \to t_n - 0$ (see Estimate (A18)). All other functions in this integrand, including the unknown function $\varphi(t)$, are assumed continuous. Hence, we can write:

$$\int_{t_{n-1}}^{t_n} [\mu_0(\tau) - h_1(\tau)\varphi(\tau)]\, G(t_n;\tau;1)\,\mathrm{d}\tau$$

$$\approx \left\{\mu_0(\tau_n) - h_1(\tau_n)\frac{\varphi(t_n) + \varphi(t_{n-1})}{2}\right\} \int_{t_{n-1}}^{t_n} G(t_n;\tau;1)\,\mathrm{d}\tau \, . \qquad (A24)$$

In view of Series (2.53) we can write:

$$\int_{t_{n-1}}^{t_n} G(t_n;\tau;1)\,\mathrm{d}\tau$$

$$= \; 2 \sum_{m=1}^{\infty} \frac{{}_m^2}{h_0^2 + h_0 + {}_m^2} \int_{t_{n-1}}^{t_n} \frac{1}{R_d^2(\;)} \exp\left[\frac{{}_m^2}{R_{d0}} \left(\frac{1}{R_d(t_n)} \quad \frac{1}{R_d(\;)} \right) \right] d$$

$$= \; 2 \sum_{m=1}^{\infty} \frac{{}_m^2}{h_0^2 + h_0 + {}_m^2} \frac{1}{{}_m^2} \exp\left[\frac{{}_m^2}{R_{d0}} \left(\frac{1}{R_d(t_n)} \quad \frac{1}{R_d(\;)} \right) \right] \Bigg|_{=t_{n-1}}^{=t_n}$$

$$= \; 2 \sum_{m=1}^{\infty} \frac{{}_m^2}{h_0^2 + h_0 + {}_m^2} \frac{1}{{}_m^2} \left(1 \quad \exp\left[\frac{{}_m^2}{R_{d0}} \left(\frac{1}{R_d(t_n)} \quad \frac{1}{R_d(t_{n-1})} \right) \right] \right)$$

$$= \; 2 \sum_{m=1}^{\infty} \frac{1}{h_0^2 + h_0 + {}_m^2} \left(1 \quad \exp\left[\frac{{}_m^2 \; t}{R_d(t_n) R_d(t_{n-1})} \right] \right)$$

$$= \; \frac{1}{1 + h_0} + 2 \sum_{m=1}^{\infty} \frac{1}{h_0^2 + h_0 + {}_m^2} \exp\left[\frac{{}_m^2 \; t}{R_d(t_n) R_d(t_{n-1})} \right] \quad g_n. \qquad (A25)$$

If $h_0 = 0$ then ${}_m = \; (m \quad (1/2))$ in series (A25). The combination of Formulae (A23) – (A25) allows us to present the discretised form of Equation (A21) (Equation (A22)) as follows:

$$(t_n) = V(t_n; 1) \quad f \;\; {}_0(\;{}_n) \quad h_1(\;{}_n)\,[\;\; (t_n) + \;\; (t_{n-1})]/2g\,g_n$$

$$\sum_{j=1}^{n-1} f \;\; {}_0(\;{}_j) \quad h_1(\;{}_j)\,[\;\; (t_j) + \;\; (t_{j-1})]/2g\,G(t_n; \;{}_j; 1) \quad t; \qquad (A26)$$

where $n = 1, 2, \ldots, N$, and g_n is given by Series (A25).

Equation (A26) can be rearranged to the form particularly convenient for the numerical analysis:

$$(t_n) = \frac{1}{1 \quad 0.5 h_1(\;{}_n) g_n} \left(V(t_n; 1) \quad \left[{}_0(\;{}_n) \quad \frac{h_1(\;{}_n) \;\; (t_{n-1})}{2} \right] g_n \right.$$

$$\left. \sum_{j=1}^{n-1} f \;\; {}_0(\;{}_j) \quad h_1(\;{}_j)\,[\;\; (t_j) + \;\; (t_{j-1})]/2g\,G(t_n; \;{}_j; 1) \quad t \right\} . \qquad (A27)$$

For $n = 1$ the sum in Formula (A27) is equal to zero and (t_0) is a known constant (see above). This allows us to calculate (t_1) explicitly using Formula (A27). Once (t_1) has been calculated we can use Formula (A27) for calculation of (t_2) etc. At the nth step, Formula (A27) is used for calculation of (t_n) using the values of (t_0), (t_1), ... (t_{n-1}) calculated at the previous steps. At this step all terms in the sum $\sum_{j=1}^{n-1}$ are already known.

Once we have obtained the numerical solution to the integral equation (2.51) we are in a position to calculate numerically function $W(t; \;)$ using its integral representation (2.49), where:

$$\hat{}_0(t) = \;{}_0(t) \quad h_1(t) \;\; (t).$$

Using the same discretisation by t and as above, we can present the discretised form of this representation as:

$$W(\hat{t}; \;) = V(\hat{t}; \;) \quad \sum_{j=1}^{N} \int_{t_{j\;1}}^{t_j} \hat{\;}_0(\;) G(\hat{t}; \;;\;) \mathrm{d}$$

$$= V(\hat{t}; \;) \quad \sum_{j=1}^{N\;1} \frac{\hat{\;}_0(t_{j\;1}) + \hat{\;}_0(t_j)}{2} G(\hat{t}; \;_j; \;) \; t \quad \frac{\hat{\;}_0(t_{N\;1}) + \hat{\;}_0(t_N)}{2}$$

$$\int_{t_{N\;1}}^{t_N} G(t_N; \;;\;) \mathrm{d} \, : \qquad (A29)$$

Note that $t_N = \hat{t}$. If $N = 1$ then the sum in Equation (A29) is equal to zero. The last integral in Equation (A29) is improper and needs to be calculated separately. Remembering the de nition of $G(t; \;;\;)$, and almost repeating the derivation of Equation (A25), we can write:

$$\int_{t_{N\;1}}^{t_N} G(t_N; \;;\;) \mathrm{d} \quad = \quad 2 \sum_{m=1}^{\infty} \frac{h_0^2 + \;_m^2}{h_0^2 + h_0 + \;_m^2} \frac{\sin \;_m \sin \;_m}{\;_m^2}$$

$$\left(1 \quad \exp \left[\frac{\;_m^2 \; t}{R_d(t_N) R_d(t_{N\;1})} \right] \right)$$

$$= \quad \frac{}{1 + h_0} + 2 \sum_{m=1}^{\infty} \frac{h_0^2 + \;_m^2}{h_0^2 + h_0 + \;_m^2} \frac{\sin \;_m \sin \;_m}{\;_m^2} \exp \left[\frac{\;_m^2 \; t}{R_d(t_N) R_d(t_{N\;1})} \right] :$$

Having substituted the latter equation into (A29), and remembering the de nition of $\hat{\;}_0(t_j)$, we obtain the required value of $W(\hat{t}; \;)$.

Appendix 3

Numerical solution of the integral Equation (3.10)

Remembering Equations (3.6) and (3.8) we can rewrite Equation (3.10) as:

$$(t) + \int_0^t (\;) \left\{ \frac{1}{\sqrt{\;\; t}} \;(t; \;) + !(t; \;) \right\} \mathrm{d} \quad = 2 \;_0(t); \qquad (A31)$$

where:

$$(t; \;) = \frac{1}{\sqrt{\;}} \left\{ \frac{1}{2\sqrt{\;}} \frac{R_d(t) \quad R_d(\;)}{t} + \sqrt{\;} H(t) \right\}$$

$$\exp \left[(R_d(t) \right.$$

(1]TJ626 Tf 19.876 17 Td [( )]TJ/FTd d [1.9552 T23 7.9701 Tf 0 -7.294 Td [(m9.388.9552 Tf 8.025 -17.534 Td [(320

$$\exp\left[-\frac{(R_d(t)+(R_d(\;))^2}{4\;(t\;\;)}\right];\tag{A33}$$

Functions $(t;\;)$ and $\omega(t;\;)$ are continuous for $\;\in[0;t]$. Hence, the singularity $1/\sqrt{t\;\;}$ of the kernel in Equation (A31) is presented in an explicit form.

We look for the solution of Equation (A31) for $t\in[0;\hat{t}]$, where $\hat{t}\;\;t_e$ is an arbitrary, but xed positive constant. Let $\;t=\hat{t}/N$ and $t_n=n\;t$, where N is the total number of time steps, $n=0;1;\ldots;N$ is the number of the current time step. Note that $t_0=0$ and $t_N=\hat{t}$. Discretisation of Equation (A31) gives:

$$(t_n)+\sum_{j=1}^{n}\int_{t_{j-1}}^{t_j}(\;)\left\{\frac{(t_n;\;)}{\sqrt{t_n\;\;}}+\omega(t_n;\;)\right\}d\;=2\;_0(t_n);\tag{A34}$$

where $n=0;1;\ldots;N$. Note that

$$(t_0)=\;(0)=2\;_0(0)$$

is the known constant derived in Appendix 5.

The rst $(n-1)$ terms in the sum in Equation (A34) can be approximated as:

$$\int_{t_{j-1}}^{t_j}(\;)\left\{\frac{(t_n;\;)}{\sqrt{t_n\;\;}}+\omega(t_n;\;)\right\}d\;$$
$$\frac{(t_j)+\;(t_{j-1})}{2}\left\{\frac{(t_n;\;_j)}{\sqrt{t_n\;\;_j}}+\omega(t_n;\;_j)\right\}\;t;\tag{A35}$$

where $j=1;2;\ldots;n-1$; $\;_j=t_j-\frac{\;t}{2}$. This approximation is valid since all functions in the integrand are continuous, and we look for the solution in the class of continuous functions ($\;(t)$ should be continuous for $t\;\;0$). In this approximation the known functions are taken at the points $\;=\;_j$ (middle of the time interval $[t_{j-1};t_j]$), while the unknown function is taken as an arithmetic mean of its values at the times t_{j-1} and t_j.

The last term in the sum in Equation (A34) has an integrable singularity $1/\sqrt{t\;\;}$ when $\;\to t\;\;0$ (recall that functions $(t;\;)$ and $\omega(t;\;)$ are continuous for $\;\in[0;t]$). This allows us to approximate this term as:

$$\int_{t_{n-1}}^{t_n}(\;)\left\{\frac{(t_n;\;)}{\sqrt{t_n\;\;}}+\omega(t_n;\;)\right\}d\;$$
$$\frac{(t_n)+\;(t_{n-1})}{2}\left[(t_n;\;_n)\int_{t_{n-1}}^{t_n}\frac{d\;}{\sqrt{t_n\;\;}}+\omega(t_n;\;_n)\;t\right]$$

$=\;\;(t_n\;\;(=$

where

$$g_n = \quad (t_n; \quad _n)\sqrt{\quad t} + \frac{!\,(t_n; \quad _n) \quad t}{2}$$

latter equation which will enable us to simplify the notation. Let us rewrite this equation as:

$$v(R;\hat{t}) = \sum_{j=1}^{N} \int_{t_{j-1}}^{t_j} (\ )G(\hat{t},\ ;R)d\ ; \qquad \text{(A41)}$$

where $\hat{t} = t_N$, $t_n = n\ t$, $n = 0;1;2;::::N$, $t = \hat{t}=N$. In all integrals we can replace $(\ )$ with the average values over the corresponding time interval $(t_{j-1}) + (t_j))=2$. Moreover, in all integrals, except the last one, we can replace $G(\hat{t},\ ;R)$ with $G(\hat{t},\ _j;R)$, where $_j = (t_{j-1} + t_j)=2$. As a result, Equation (A41) can be presented in a more explicit form:

$$v(R;\hat{t}) = \sum_{j=1}^{N-1} \frac{(t_{j-1}) + (t_j)}{2} G(\hat{t},\ _j;R)\ t + \frac{(t_{N-1}) + (t_N)}{2} \int_{t_{N-1}}^{t_N} G(\hat{t},\ ;R)d\ : \qquad \text{(A42)}$$

Firstly we assume that an *a priori* chosen R is not equal to $R_d(\hat{t})$. In this case $G(\hat{t},\ ;R)$, as defined by Equation (3.6), approaches 0, when $\ ! \ \hat{t}\ \ 0$. Hence the singularity in the integrand is not present and the last time step can be treated as

Appendix 5

Derivation of the expression for $_0(0)$

Having substituted Equation (3.20) into Equation (3.19) and integrating by parts we obtain:

$$U_R^0(t;R)\Big|_{R=R_d(t)} = \int_0^{R_e} (\ T_{d0}(\ ))\ \frac{\partial G_1(t;R;\ )}{\partial\ }\Big|_{R=R_d(t)} d$$

$= (\ T_{do}($

$$f_n \approx \mu_0(0) - (-1)^{n;0} D_l \lambda_n^2 \int_0^t \frac{1}{R_d(\tau)^2} \exp\left[(-1)^{n;0}\frac{D_l\lambda_n^2}{R_{d0}}\left(\frac{1}{R_d(t)}-\frac{1}{R_d(\tau)}\right)\right] d\tau \;. \tag{A61}$$

$\mu_0(\tau)$ in the integrand of (4.41) is taken at the beginning of the time step.

Remembering that

$$d(R_d(\tau)^{-1}) = -\frac{R_d'}{R_d^2(t)} d\tau$$

we can rearrange the last term in (A61) to

$$(-1)^{n;0} D_l \lambda_n^2 \int_0^t \frac{1}{R_d(\tau)^2} \exp\left[(-1)^{n;0}\frac{D_l\lambda_n^2}{R_{d0}}\left(\frac{1}{R_d(t)}-\frac{1}{R_d(\tau)}\right)\right] d\tau =$$

$$\frac{(-1)^{n;0} D_l\lambda_n^2}{R_d'} \exp\left[(-1)^{n;0}\frac{D_l\lambda_n^2}{R_{d0}}\left(\frac{1}{R_d(t)}\right)\right] \int_0^t \frac{R_d'}{R_d(\tau)^2} \exp\left[-(-1)^{n;0}\frac{D_l\lambda_n^2}{R_{d0}}\left(\frac{1}{R_d(\tau)}\right)\right] d\tau =$$

$$\frac{(-1)^{n;0} D_l\lambda_n^2}{R_d'} \exp\left[(-1)^{n;0}\frac{D_l\lambda_n^2}{R_{d0}}\left(\frac{1}{R_d(t)}\right)\right] \left(\frac{R_{d0}}{(-1)^{n;0} D_l\lambda_n^2}\right)\left[\exp\left(-(-1)^{n;0}\frac{D_l\lambda_n^2}{R_{d0}}\left(\frac{1}{R_d(t)}\right)\right) - \exp\left(-(-1)^{n;0}\frac{D_l\lambda_n^2}{R_{d0}}\left(\frac{1}{R_d(0)}\right)\right)\right]$$

$$= 1 - \exp\left[(-1)^{n;0}\frac{D_l\lambda_n^2}{R_{d0}}\left(\frac{1}{R_d(t)}-\frac{1}{R_d(0)}\right)\right] = 1 - \exp\left[-(-1)^{n;0}\frac{D_l\lambda_n^2 t}{R_{d0}R_d(t)}\right] \;. \tag{A62}$$

When deriving (A62) we took into account (2.8).

Having substituted (A62) into (A61), we obtain (4.42).

Appendix 7

Derivation of Formula (5.9)

Introducing a new variable

$$u = (T - T_{g0}(R_g))\, R$$

we can simplify Equation (5.1) and initial and boundary conditions (5.3) – (5.4) to:

$$\frac{\partial u}{\partial t} = \kappa \frac{\partial^2 u}{\partial R^2} + RP(t;R); \tag{A71}$$

$$u|_{t=0} = \tilde{T}_0 R \tag{A72}$$

$$u|_{R=R_b^-} = u|_{R=R_b^+}\,;\quad k_b\left[R_b u_R' - u\right]_{R=R_b^-} = k_g\left[R_b u_R' - u\right]_{R=R_b^+}\,;\quad u|_{R=R_g} = 0\,; \tag{A73}$$

where

$$T_0 \equiv T_0(R) = \begin{cases} T_{g0}(R_g) - T_{b0}(R) & \text{when } R \le R_b \\ T_{g0}(R_g) - T_{g0}(R) & \text{when } R_b < R \le R_g; \end{cases}$$

Conditions (A73) need to be amended by the boundary condition at $R = 0$. Since $T - T_{g0}$ is finite at $R = 0$ then $u|_{R=0} = 0$.

We look for the solution of Equation (A71) in the form:

$$u = \sum_{n=1}^{\infty} \theta_n(t) v_n(R), \tag{A74}$$

where functions $v_n(R)$ form the full set of non-trivial solutions of the eigenvalue problem:

$$\frac{\mathrm{d}^2 v}{\mathrm{d}R^2} + a^2 \lambda^2 v = 0 \tag{A75}$$

subject to boundary conditions:

$$\left.\begin{aligned} & v|_{R=0} = v|_{R=R_g} = 0 \\ & v|_{R=R_b^-} = v|_{R=R_b^+} \\ & k_b \left[R_b v'_R - v\right]_{R=R_b^-} = k_g \left[R_b v'_R - v\right]_{R=R_b^+} \end{aligned}\right\}, \tag{A76}$$

where

$$a = \frac{1}{\sqrt{\kappa}} = \begin{cases} \sqrt{\frac{c_b \rho_b}{k_b}} \equiv a_b & \text{when } R \le R_b \\ \sqrt{\frac{c_{pg} \rho_g}{k_g}} \equiv a_g & \text{when } R_b < R \le R_g. \end{cases} \tag{A77}$$

Note that λ has dimension $1/\sqrt{\text{time}}$. We look for the solution of Equation (A75) in the form:

$$v(R) = \begin{cases} A \sin(\lambda a_b R) & \text{when } R \le R_b \\ B \sin(\lambda a_g (R - R_g)) & \text{when } R_b < R \le R_g. \end{cases} \tag{A78}$$

Function (A78) satisfies boundary conditions (A76) at $R = 0$. Having substituted function (A78) into boundary conditions (A76) at $R = R_b$ we obtain:

$$A \sin(\lambda a_b R_b) = B \sin(\lambda a_g (R_b - R_g)); \tag{A79}$$

$Ak_b\,[R_b \lambda a_b \cos(\lambda a_b R_b)$ a b ba cos(a F18 11.9552 Tf 54285u2 0 Td [(R)]TJm72in(

$$= \frac{c_b \;\; {}_b R_b}{2\sin^2(\;\; {}_n a_b R_b)} + \frac{c_{pg} \;\; {}_g (R_g \quad R_b)}{2\sin^2(\;\; {}_n a_g (R_b \quad R_g))} \quad \frac{k_b \quad k_g}{2R_b \;\; {}^2_n}: \qquad (A715)$$

and the expression for $\theta_n(0)$ can be further simplified to:

$$\theta_n(0) = \frac{c_b \rho_b T_0}{||v_n||^2 \sin(\lambda_n a_b R_b)} \int_0^{R_b} R \sin(\lambda_n a_b R) \mathrm{d}R = \frac{T_0 \sqrt{k_b c_b \rho_b}}{\lambda_n ||v_n||^2} \left(R_b \cot(\lambda_n a_b R_b) - \frac{1}{\lambda_n a_b} \right). \qquad (A7\,20)$$

The solution of Equation (A7 18) subject to the initial condition (A7 20) can be written as:

$$\theta_n(t) = \exp\left(-\lambda_n^2 t\right) \theta_n(0) + \int_0^t \exp\left(-\lambda_n^2 (t-\tau)\right) p_n(\tau) \mathrm{d}\tau. \qquad (A7\,21)$$

Equation (5.9) follows from the definition of u and Equations (A7 4) and (A7 21).

Appendix 8

Proof of orthogonality of $v_n(R)$ with the weight b

Remembering Expressions (A7 14) for $v_n(R)$ we can write for $n \neq m$:

$$I_{nm} \equiv \int_0^{R_g} v_n(R) v_m(R) b \mathrm{d}R = \frac{k_b a_b^2}{\sin(\lambda_n a_b R_b)\sin(\lambda_m a_b R_b)} \int_0^{R_b} \sin(\lambda_n a_b R)\sin(\lambda_m a_b R)\mathrm{d}R$$

$$+ \frac{k_g a_g^2}{\sin(\lambda_n a_g(R_b - R_g))\sin(\lambda_m a_g(R_b - R_g))} \int_{R_b}^{R_g} \sin(\lambda_n a_g(R - R_g))\sin(\lambda_m a_g(R - R_g))\mathrm{d}R$$

$$= \frac{k_b a_b^2}{2\sin(\lambda_n a_b R_b)\sin(\lambda_m a_b R_b)} \left[\frac{\sin((\lambda_n - \lambda_m) a_b R_b)}{(\lambda_n - \lambda_m) a_b} - \frac{\sin((\lambda_n + \lambda_m) a_b R_b)}{(\lambda_n + \lambda_m) a_b} \right]$$

$$- \frac{k_g a_g^2}{2\sin(\lambda_n a_g(R_b - R_g))\sin(\lambda_m a_g(R_b - R_g))} \left[\frac{\sin((\lambda_n - \lambda_m) a_g (R_b - R_g))}{(\lambda_n - \lambda_m) a_g} - \frac{\sin((\lambda_n + \lambda_m) a_g (R_b - R_g))}{(\lambda_n + \lambda_m) a_g} \right]$$

$$= \frac{1}{2(\lambda_n - \lambda_m)} \left[\frac{k_b a_b \sin((\lambda_n - \lambda_m) a_b R_b)}{\sin(\lambda_n a_b R_b)\sin(\lambda_m a_b R_b)} - \frac{k_g a_g \sin((\lambda_n - \lambda_m) a_g (R_b - R_g))}{\sin(\lambda_n a_g(R_b - R_g))\sin(\lambda_m a_g(R_b - R_g))} \right]$$

$$+ \frac{1}{2(\lambda_n + \lambda_m)} \left[-\frac{k_b a_b \sin((\lambda_n + \lambda_m) a_b R_b)}{\sin(\lambda_n a_b R_b)\sin(\lambda_m a_b R_b)} + \frac{k_g a_g \sin((\lambda_n + \lambda_m) a_g (R_b - R_g))}{\sin(\lambda_n a_g(R_b - R_g))\sin(\lambda_m a_g(R_b - R_g))} \right]$$

$$= \frac{[k_b a_b (\cot(\lambda_m a_b R_b) - \cot(\lambda_n a_b R_b)) - k_g a_g (\cot(\lambda_m a_b (R_b - R_g)) - \cot(\lambda_n a_b (R_b - R_g)))]}{2(\lambda_n - \lambda_m)}$$

$$+ \frac{[-k_b a_b (\cot(\lambda_m a_b R_b) + \cot(\lambda_n a_b R_b)) + k_g a_g (\cot(\lambda_m a_b (R_b - R_g)) + \cot(\lambda_n a_b (R_b - R_g)))]}{2(\lambda_n + \lambda_m)}$$

Remembering Equation (A7 13) we can write:

$$I_{nm} = \frac{1}{2(\lambda_n - \lambda_m)} \left(\frac{k_b - k_g}{R_b \lambda_m} - \frac{k_b - k_g}{R_b \lambda_n} \right) - \frac{1}{2(\lambda_n + \lambda_m)} \left(\frac{k_b - k_g}{R_b \lambda_m} + \frac{k_b - k_g}{R_b \lambda_n} \right)$$

$$= \frac{k_b - k_g}{2R_b \lambda_n \lambda_m} - \frac{k_b - k_g}{2R_b \lambda_n \lambda_m} = 0.$$